Granular Matter (2022) 24:41
https://doi.org/10.1007/s10035-021-01189-0

ORIGINAL PAPER

Effects of particle morphology on the minimum and maximum void ratios of granular materials

M. Ali Maroof[1] · Ahmad Mahboubi[1] · Eric Vincens[2] · Ali Noorzad[1]

Received: 7 June 2021 / Accepted: 9 November 2021 / Published online: 24 January 2022

Abstract
The minimum and maximum void ratios (e_{min} and $e_{max,}$ respectively) of soils are intrinsic soil properties related to their particle size distribution (PSD) and particle shape. Different attempts have been made to predict these reference void ratios for cohesionless soils through the involved particle morphology. However, these predictive models do not handle flaky and elongated particles. Besides, these kinds of models just consider the particle shape throughout a two-dimensional analysis. In this current study, experimental work has been carried out on particles with five different geological and morphological properties and nine different gradations. The particle shape effect involves glass beads, rounded, angular, flaky, and elongated particles to expand both the range of particle sphericity and roundness. A wide range of particle sizes, including uniformly distributed, widely distributed, and upward concave graded soils were chosen. Particle sphericity and roundness were measured by micro CT images and image processing. Furthermore, a comprehensive database was gathered based on past experimental results from the literature. This database was used to derive the predictive equations for determining $e_{min,}$ e_{max}, and the void ratio range (e_{max}-e_{min}), considering sphericity, roundness, and uniformity coefficient. The developed new formulas show good agreement with the current and past experimental results.

Keywords Maximum void ratio · Minimum void ratio · Particle morphology · Roundness · Sphericity

1 Introduction

The key parameter to provide a comprehensive understanding of particle assemblies' behavior can be directly or indirectly associated with particle packing and density characteristics for design and production processes in many areas including metallurgical, pharmaceutical, mineral industries, and geotechnical engineering. Relative density is one of the most important properties that can influence the mechanical behavior of granular soils, but the particle shape may also greatly monitor this behavior [1]. More precisely, relative density influences the physical properties, particle packing, compressibility, the mechanical behavior together with the stress–strain relationships, permeability, liquefaction, and suffusion susceptibility of granular materials [2], [3], [4], [5], [6], [7].

The densest and the loosest packing of particles of granular material are controlled by some intrinsic properties such as the particle size distribution (PSD), the mean particle size, the particle shapes, and the method of packing (particle arrangement) [8], [9], [10], [11], [12], [13], [14].

Generally, the minimum and maximum void ratios increase when roundness, sphericity, and the coefficient of uniformity decrease [8, 9, 11, 15].

The grain assemblies composed of several fractions are more easily compacted than other soils with a uniform distribution [16]. At a given compaction effort, the limit void ratios (e_{max} and e_{min}) of a collection of particles having various sizes are lower than that of uniformly distributed soils [17–19]. So, the limit void ratios are a function of the grain

✉ Ahmad Mahboubi
a_mahboubi@sbu.ac.ir; ahmad.mahboubi@gmail.com

M. Ali Maroof
m_maroof@sbu.ac.ir

Eric Vincens
eric.vincens@ec-lyon.fr

Ali Noorzad
a_noorzad@sbu.ac.ir

1 Faculty of Civil, Water and Environmental Engineering, Shahid Beheshti University, 1658953571 Tehran, Iran

2 Ecole Centrale de Lyon, LTDS-G8, 36, Av Guy de Collongue, 69134 Ecully, France

size distribution and thus a function of the coefficient of uniformity [8].

The limit void ratios of a cohesionless soil also depend on its particle sizes [20]. However, different diameters were proposed to characterize the effective size of heterodisperse samples such as D_{10} and D_{50} [17], but the latter one is the most used one. Fine sand with a higher D_{50} leads to a higher e_{min} but a lower e_{max} [21]. Indeed, inter-particle attractive forces of non-plastic fines may affect the packing of the material at its extreme states [22]. However, for particles larger than 0.2 mm, the particle size has a negligible impact on the density limits [17], and the PSD shape and particle shape (particle morphology) are the main parameters that may affect the limit void ratios.

The particle shape also influences the soil fabric and, as a consequence, the limit void ratios. The particle shape can be divided into three categories: macro, medium, and micro scales associated with form/sphericity, roundness, and finally roughness [23], [24], [25].

The form describes the overall shape of particles and is characterized by sphericity and form [26]. Sphericity is defined as the ratio of the surface area of the equivalent sphere having the same volume as the grain to the grain surface area. Moreover, particle form is also described by flatness and elongation ratios in 3 different planes [27], [28].

Roundness, which is defined in a plane, evaluates whether the edges and corners are sharp or curved [29]. It is defined as the average radius of edge curvature divided by the inscribed circle and is classified by Powers' class [30]. This scale grades the roundness according to six classes: very angular, angular, sub-angular, sub-rounded, rounded, and well rounded. The surface roughness is the smallest scale observation. Besides, both sphericity and roundness may be quantified by a single parameter, the particle regularity, ρ, defined as the mean value of sphericity and roundness, $\rho = (R + S)/2$ [10].

Moreover, different numerical investigations have been performed in order to study the particle packing characterization. Some attempts have been made by researchers to tackle this topic of particle shape and grading effect on the packing characteristics and on the compressibility using numerical methods both discrete element method (DEM) [31, 32], and combined finite-discrete element method (FDEM) [33], [34].

The values for the loosest and densest states may vary depending on the sample preparation and the test methods. There are various methods for measuring the minimum density and a reliable method for maximum dry density measurement would be significantly needed [6], [35]. Besides, the geotechnical characteristics of the coarse granular materials such as coarse gravel, rockfill, and rock from mining works, are difficult either in sampling or laboratory testing due to oversize particles [21]. Consequently, estimating the limit void ratios or limit dry densities of these materials directly from physical properties can be very useful, particularly for granular material containing oversized particles like quarry and rockfill. Meanwhile, various uniformity indexes derived from approaches to characterizing fragmentation such as Andreev-Gaudin-Schuhman law, Rosin–Rammler, and power law [36], have a conversion from *Cu* in lognormal distribution.

The quantitative correlation of these parameters and the proposed models in this research area have been reviewed in the next section.

2 Previously proposed relationships for the limit void ratios and the void ratio range

The loosest state for packing of mono-size spheres can be geometrically obtained in a cubic packed arrangement with the coordination number (CN) equal to six and $e_{max} = 0.92$. The densest packing is the tetrahedral or pyramidal packing of mono-size spheres with CN = 12 and $e_{min} = 0.35$. The limit void ratios for spheres associated with a widely distributed gradation may significantly differ from these reference limits with values, such as $e_{max} = 0.32$ and $e_{min} = 0.19$.

There exist different proposals in the literature that relate the limit void ratios with previously mentioned grain parameters. For example, some authors proposed to find the grain-size distributions that give the smallest possible void ratio [18, 37, 38]. The particle shape is considered as a constant number that was assumed to be equal to 0.6, 0.73, and 1.00 for spherical, natural sand and gravel, and crushed particles, respectively [18]. An empirical formula was proposed to predict the maximum and minimum dry densities regarding the characteristic particle size d_{10}, the PSD curve, and particle sphericity [39]. Furthermore, several charts have been provided for determining the limit void ratios in clean sands with normal to moderately skewed PSD curves [8]. The proposed charts depend only on the PSD curve shape by means of the coefficient of uniformity (*Cu*) and Wadell's roundness. Some equations approximate these charts to determine e_{max} and e_{min} values for sand and gravel samples as a function of *Cu* and *R* values [6, 40]. Two relationships have also been suggested for granular soils with $Cu < 2.5$ to obtain that the limit void ratios are based on roundness solely [11]. In these relationships, the effect of grain shape is not clearly specified, and only the influence of roundness is considered.

For natural sands with $Cu < 2.5$, an empirical equation was proposed involving the particle regularity, ρ [10]. A two-variable equation was proposed for uniform sands that involves the roundness *R* and mean particle size D_{50} [41]. A methodology was also suggested for obtaining e_{max} and e_{min} considering the shape of the particles with sphericity and roundness [42]. Afterward, these researchers amended their relationships with more data and proposed relationships involving R, S, Cu, e°_{max}, and e°_{min} [13]. Where e°_{max} and e°_{min} are the maximum and minimum void ratios for the glass spheres with $Cu = 1$, respectively ($R = S = C_u = 1.0$). Moreover, multivariable relationships, including the influence of the uniformity coefficient, particle regularity, and the specific gravity of the material and glass (ρ, C_u, G_m, and G_g), were suggested [43]. All of these predictive relationships are presented in Table 1.

The difference between the densest and loosest packing provides a general basis for the relative assessment of granular soil properties [15].

The range of extreme void ratios ($e_{max} - e_{min}$) may be another characteristic of sandy soil that depends on its inherent properties such as the PSD, percentage of fine particles, and particle shape [3].

The increase of the maximum void ratio associated with decreasing roundness is more noticeable than for the minimum void ratio [1]. Accordingly, the dissimilarity between the limit void ratios (e_{max}-e_{min}), decreases as the particles become rounded and spherical [44]. Furthermore, the e_{max}/e_{min} ratio was found related to Cu and the particle shape [13]. We give in Table 2 different relationships that relate e_{min} to e_{max}, that quantify (e_{max}-e_{min}) or the ratio e_{max}/e_{min} to other physical quantities such as the grading or the particle roundness.

Some of the previous researches have not separated the effects of particle size and particle morphology on the limit void ratios, and the available empirical formulas are usually single variable functions of either grain size or grain shape [41]. Moreover, in previous researches, the distinct effect of grain shape has not been clearly investigated. Indeed, these different works have only focused on investigating the effect of roundness [6, 8, 10, 38]. Some methods have evaluated the shape of the grains through visual comparison, and other methods have calculated sphericity and roundness in a two-dimensional state [13, 42, 43], while grains are three-dimensional in nature. The discrepancy of definitions for roundness and sphericity and the different used approaches do not facilitate comparing results and trends found by different authors. For these reasons, there is a need for more detailed investigations around the influence of the 3D grain shape on the limit void ratios [45].

In this study, we have described the particle shape using three-dimensional sphericity and Wadell's roundness, and their influence on e_{max} and e_{min} was evaluated. Different experiments have been carried out with different particle shapes and PSD curves to reach this goal. The soil and glass bead samples were provided by nine identical gradations and various shapes. Moreover, a database was created collecting different experimental results reported in the literature. Then several new multivariable empirical equations have

Table 2 Relationships relating the limit void ratios e_{max} and e_{min}

Predictive relations	Variables	References
$e_{max} = 1.53\ e_{min} + 0.072$	–	[15]
e_{max}-$e_{min} = 0.07R^{-1} + 0.138$		[11]
$e_{max} = 1.295\ e_{min} + 0.1697$	–	[12]
$e_{max}/e_{min} = (C_u/R)^{0.05} e^{\circ}_{max}/e^{\circ}_{min}$	R, Cu, e°_{max}, e°_{min}	[13]

Table 1 Predictive relationships for the limit void ratios, e_{max} and e_{min}

Predictive relations	Variables	References
$e_{max} = 0.65R^{-0.36}$, $e_{min} = 0.43R^{-0.28}$	R*	[43]
$e_{max} = 0.554 + 0.154R^{-1.0}$, $e_{min} = 0.359 + 0.082R^{-1.0}$	R, $Cu = 1.0$#	[44]
$e_{max} = 1.3 - 0.62R$, $e_{min} = 0.8 - 0.34R e_{max} = 1.5 - 0.82\rho, e_{min} = 0.9 - 0.44\rho$	ρ, R, $Cu < 2.50$‡	[10]
$e_{max} = 0.615 + 0.107R^{-1}$, $e_{min} = 0.433 + 0.0.051R^{-1}$	R, $Cu < 2.50$	[11]
$1/e_{max} = \left[-0.15R^3 - 14.62R^2 + 1.99R - 0.09\right] ln(C_U) + \left[4.32R^3 - 8.67R^2 + 5.96R - 0.16\right]$ $1/e_{min} = \left[7.98R^3 - 14.62R^2 + 8.85R - 0.72\right] ln(C_U) + \left[21.32R^3 - 32.95R^2 + 17.21R - 1.00\right]$	R, Cu	[6]†
$e_{min} = \left((8.05R+0.3)/(23R-2.0)\right) C_u^{\left((0.77-6.72R)/(21R-2.1)\right)}$ $e_{max} = \left((7.2R+0.4)/(12R-1.0)\right) C_u^{\left((0.65-5.49R)/(18R-1.8)\right)}$	R, Cu	[39]†
$e_{max} = 0.50R^{-0.2} + 0.41S^{-0.6} + 0.34C_u^{-0.2} - 0.51 e_{min} = 0.37R^{-0.2} + 0.28S^{-0.6} + 0.31C_u^{-0.3} - 0.48$	R, S, Cu	[41]
$e_{max} = R^{-0.20}S^{-0.25}C_u^{-0.10}e^{\circ}_{max}$, $e_{min} = R^{-0.15}S^{-0.25}C_u^{-0.15}e^{\circ}_{min}$	R, S, Cu, e°_{max}, e°_{min}	[13]
$e_{min} = 0.701 + c_u^{-0.304}$	Cu	[20]
$e_{max} = 0.619R^{-0.372}D^{-0.048}$, $e_{min} = 0.413R^{-0.291}D^{-0.043}$	R, D††	[40]
$e_{max} = 1.13e^{(0.45-0.9\rho)}C_u^{-0.172}\left(\frac{G_m}{G_g}\right)^{-0.4}$, $e_{min} = 1.17e^{(0.009-\rho)}C_u^{-0.241}\left(\frac{G_m}{G_g}\right)^{-0.4}$	ρ, Cu, G_m, G_g*†	[42]

*R = Wadell roundness, most samples were uniform sand, #) test data from Youd (1973), natural and angular uniform sands, ‡natural and crushed uniform sands, †test data from Youd (1973), ††D: The normalized grain size ($D = D_{50}/D_{ref}$, with $D_{ref} = 1$ mm), *†G_m and G_g: specific gravity of the material and glass, respectively

been developed based on this database and compared with the previous empirical formula.

3 Material and method

3.1 Particle morphology

The effect of grain shape was investigated on the minimum and maximum densities by using spherical, rounded, angular, flaky, and elongated particles. The materials used for these experiments have been carefully chosen from nine different gradations with various shapes taking into account both glass beads and soil grains with different geological and morphological properties. Glass beads and glass balletoni were used to represent the class of spherical particles. The rounded grains were provided from natural alluvial sediment while the angular grains result from the manufactured crushed aggregate. The flaky particles were taken from alluvial fans with metamorphic rocks (slate) source areas. In addition, elongated grains were derived from the residual weathered pyramid basalt. A picture of the samples and the finer fraction scanning electron microscope images (SEM) are given in Figs. 1 and 2, respectively. It is essential to mention that a few fine glass beads were not perfectly rounded and spherical, and the glass beads' sphericity and roundness were found equal to 0.96 and 0.98, respectively.

The effect of grain size has been investigated based on nine different gradations that can be qualified as widely distributed, uniform, and upwardly concave, which attempted to cover different gradations. The PSD curves are depicted in Fig. 3, and the gradation characteristics of each material are given in Table 3.

3.2 Particle shape measurement

In the current study, X-ray micro-computed tomography (micro-CT) images and 3D image processing were employed to obtain precise particle morphology. The image analysis was executed to retrieve the particle surface information via the OnDemand3D software Cybermed Inc.: Operating manual,OnDemand3D application, [46] and the 3DimViewer software Laboratory and s.r.o.:3DimViewer3.1.1, [47]. The particles' dimensions (I, L, and S), particles' surface areas (A), particles' volumes (V), inscribed and circumference spheres, and circles diameter are measured using image processing [48].

The sphericity was determined with three-dimensional information using the inscribed-circumscribed sphere sphericity, $\psi_{i-c} = \frac{d_{i-s}}{d_{c-s}}$ in which d_{i-s} and d_{c-s} are the diameters of the inscribed and circumscribed spheres, respectively. The particles' form was classified based on the sphericity classification proposed by Maroof et al. [25] that considered particles in a 3D state.

The roundness was quantified according to Wadell's method as the ratio between the average radius of the corner curvature of particle surface projection in a given plane and

Fig. 1 Images of the glass beads and soil samples. GB: glass beads, RO: rounded particles, CR: crushed angular aggregates, EL: elongated particle, FL: flaky particle

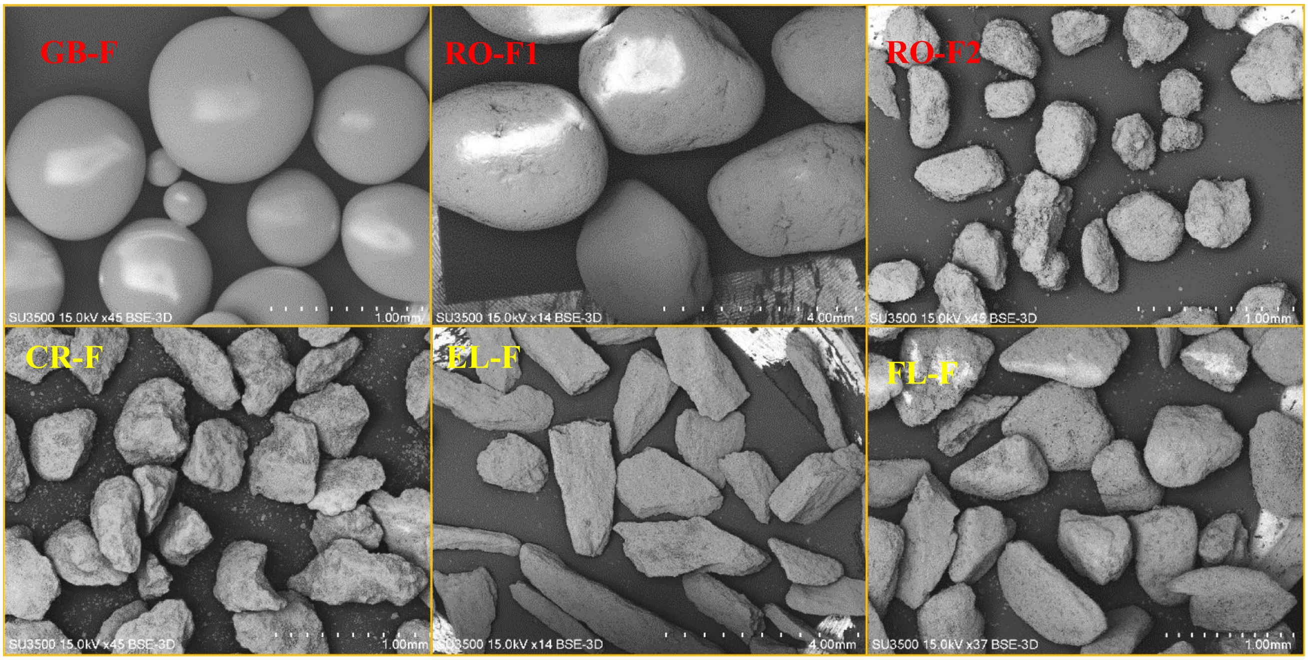

Fig. 2 SEM images of particles: GB-F (fine glass beads), RO (rounded particles- Firoozkooh sand), RO-F2 (fine alluvial rounded particle), CR-F (fine crushed aggregate), EL-F (fine elongated particle), FL-F (fine flatness particle)

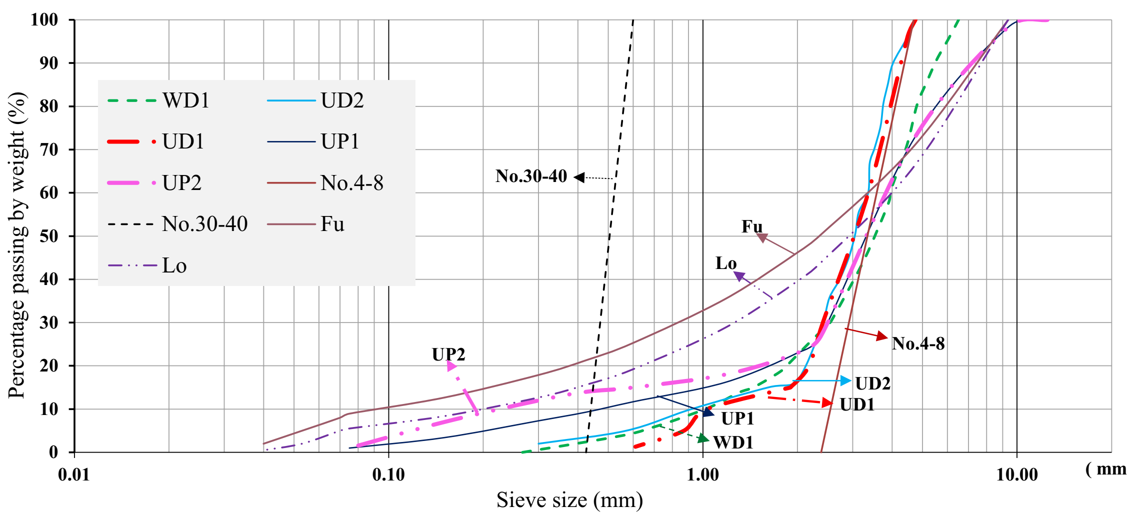

Fig. 3 Particle size distribution curve of materials

the radius of the maximum inscribed circle [26]. Particle roundness was classified based on Powers' verbal class into six classes from very angular to well rounded [30]. In this study, roundness was quantified in 2D state, sphericity is measured in 3D, and regularity, ρ is used to synthesize the average property for particle shape description.

The surface texture of the glass spheres was glassy, the surface texture of the sub-rounded and flaky particles was relatively smooth, and the angular and elongated particles had a rough texture. Table 4 gives the mean sphericity, roundness, and particle shape classification/description.

3.3 Test program

There are different procedures for the determination of densest packing (e_{min}) in cohesionless soils, including the vibrating packing method, tapping method, and vibratory tamping compaction method. Various testing procedures result in marginally different e_{min} values for a given soil [49]. For

Table 3 Index properties of the test materials

C_C	C_U	D_{90}	D_{60}	D_{30}	D_{10}	D_5	USCS classification	PSD NO	Material
0.94	1.16	0.58	0.52	0.47	0.45	0.44	*SP*	No.30–40	Glass bead, Soil
0.85	1.43	4.47	3.65	2.82	2.56	2.43	*SP*	No.4–8	Glass bead, Soil
1.68	3.26	3.99	3.36	2.41	1.03	0.83	*SP*	UD1	Glass bead, Soil
1.88	3.65	3.99	3.36	2.41	0.92	0.57	*SP*	UD2	Glass bead, Soil
1.57	3.76	5.55	3.98	2.57	1.06	0.62	*SP*	WD1	Glass bead, Soil
3.46	9.73	6.34	4.38	2.61	0.45	0.21	*SP*	UP1	Glass bead, Soil
7.58	20.8	6.34	4.38	2.61	0.21	0.15	*SP*	UP2	Glass bead, Soil
1.98	21.2	8.73	4.03	1.23	0.19	0.07	*SW*	Lo	Glass bead, Soil
2.33	36.5	8.21	3.29	0.83	0.09	0.05	*SW-SM*	Fu	Glass bead, Soil

Table 4 Mean sphericity, roundness, and particle shape classification [4]

Roughness	Roundness class	Wadell's Roundness	Flaky index	Elongation index	Sphericity class	ψ_{i-c}	Particles
Glassy	Well rounded	0.98	–	–	High sphericity	0.96	Glass beads/balletini
Relatively smooth	Rounded	0.63	–	–	Medium sphericity	0.46	Rounded particle
Rough	Angular	0.24	–	–	Low sphericity	0.37	Crushed sand
Smooth	SubAngular	0.48	0.14	–	Slab	0.14	Slate
Relatively rough	Angular	0.32	–	0.16	Discoid	0.096	Weathered pyramid basalt

sandy soils, the results of the vibratory method lead to significantly greater values than, for example, the one obtained by the standard Proctor compaction tests [50]. The vibrating table method, ASTM D4253 [35], is the common testing method for cohesionless soils with up to 15% fine content. However, one disadvantage of the vibratory table method is a slight particle breakage for angular soils [49], which in general holds true for elongated, flaky, and crushed sands. In the current study, this method was used for the measurement of e_{min}.

ASTM D4254 suggests three procedures to determine e_{max}; the funnel pouring method, extracting a soil-filled tube, and inverting a graduated cylinder [51] which was used herein to determine e_{max}. The sand was deposited in the mold using a funnel while keeping the dropping height small, and a spiral movement was performed to minimize particle segregation.

In this study, the collected samples were categorized into five different particle shapes with nine gradations. A total of 45 samples, with different geological and morphological properties, were prepared and tested.

4 Results and discussions

4.1 Experimental results

Table 5 provides the required information about the samples with various morphologies, including the particle gradation, particle shape, and particle packing characteristics.

Nine types of sands with identical PSD and five particle shapes were selected. The dependency of the limit void ratios concerning *Cu* is depicted in.

Figure 4a, b according to the regularity coefficient. The observed tendency was expected since, for broadly graded soils, the finer fraction may fill the voids between the coarser fraction skeleton. Similar graphs were previously first suggested by Youd [8], which related the limit void ratios to *Cu* and *R*, but were also proposed by other researchers more recently [6], [13], [40].

The dependency of the limit void ratios with respect to the regularity factor is given in Fig. 5. As shown in the figure, a decrease in particle regularity leads to a nonlinear increase of both e_{max} and e_{min}. The results demonstrate the nonlinear trend of the low sphericity and angular particles, which gradually become linear for more spherical and rounded particles ($\rho > 0.6$).

Table 5 test results for samples with various morphologies

Particle gradation		Particle shape			Particle packing	
PSD	C_u	Sphericity, S	Roundness, R	Regularity, ρ	e_{max} †	e_{min} ‡
No.30–40	1.16	0.97	0.96	0.97	0.65	0.50
	1.16	0.62	0.73	0.68	0.76	0.52
	1.16	0.51	0.4	0.46	1.09	0.71
	1.16	0.1	0.66	0.38	1.17	0.73
	1.16	0.12	0.17	0.15	1.72	1.13
No.4–8	1.43	0.97	0.96	0.97	0.63	0.47
	1.43	0.62	0.73	0.68	0.73	0.52
	1.43	0.51	0.4	0.46	1.02	0.72
	1.43	0.1	0.66	0.38	1.11	0.79
	1.43	0.12	0.17	0.15	1.67	1.09
UD1	3.26	0.97	0.96	0.97	0.52	0.40
	3.26	0.62	0.73	0.68	0.58	0.39
	3.26	0.51	0.4	0.46	0.79	0.49
	3.26	0.1	0.66	0.38	0.93	0.50
	3.26	0.12	0.17	0.15	1.41	1.03
UD2	3.65	0.97	0.96	0.97	0.47	0.38
	3.65	0.62	0.73	0.68	0.55	0.39
	3.65	0.51	0.4	0.46	0.76	0.53
	3.65	0.1	0.66	0.38	0.82	0.59
	3.65	0.12	0.17	0.15	1.13	0.77
WD1	3.8	0.97	0.96	0.97	0.50	0.41
	3.8	0.62	0.73	0.68	0.60	0.42
	3.8	0.51	0.4	0.46	0.78	0.53
	3.8	0.1	0.66	0.38	0.87	0.55
	3.8	0.12	0.17	0.15	1.24	0.85
UP1	9.7	0.97	0.96	0.97	0.50	0.27
	9.7	0.62	0.73	0.68	0.51	0.29
	9.7	0.51	0.4	0.46	0.69	0.40
	9.7	0.1	0.66	0.38	0.79	0.47
	9.7	0.12	0.17	0.15	1.32	0.73
UP2	20.8	0.97	0.96	0.97	0.48	0.27
	20.8	0.62	0.73	0.68	0.50	0.29
	20.8	0.51	0.4	0.46	0.70	0.42
	20.8	0.1	0.66	0.38	0.81	0.48
	20.8	0.12	0.17	0.15	1.28	0.70
Lo	21.2	0.97	0.96	0.97	0.37	0.22
	21.2	0.62	0.73	0.68	0.49	0.28
	21.2	0.51	0.4	0.46	0.61	0.32
	21.2	0.1	0.66	0.38	0.70	0.35
	21.2	0.12	0.17	0.15	1.16	0.70
Fu	36.5	0.97	0.96	0.97	0.35	0.19
	36.5	0.62	0.73	0.68	0.48	0.21
	36.5	0.51	0.4	0.46	0.59	0.28
	36.5	0.1	0.66	0.38	0.66	0.34
	36.5	0.12	0.17	0.15	0.93	0.56

† ASTM D4253 ‡ ASTM D4254

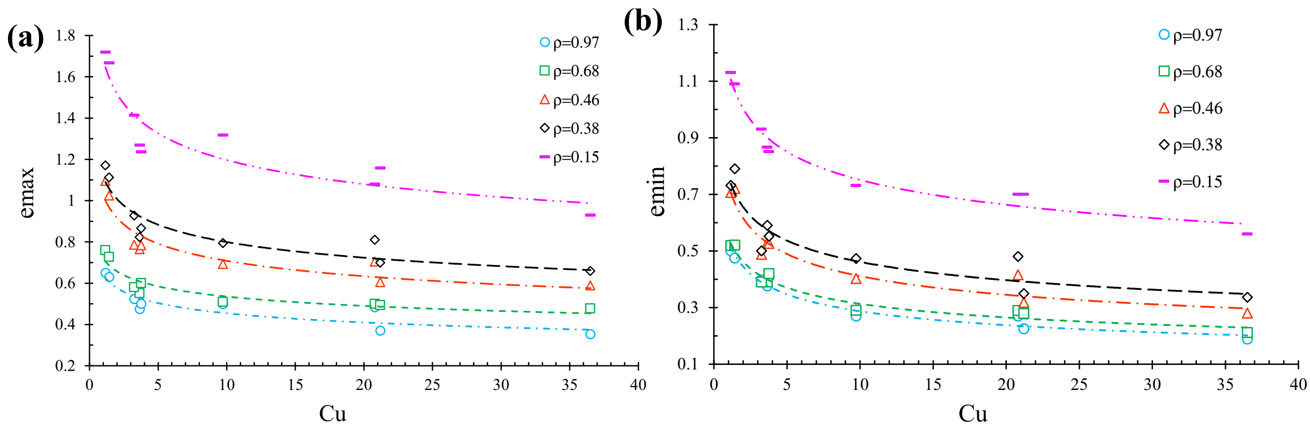

Fig. 4 Void ratio limits as a function of *Cu* for samples with different particle shapes (a: e_{max}, b: e_{min})

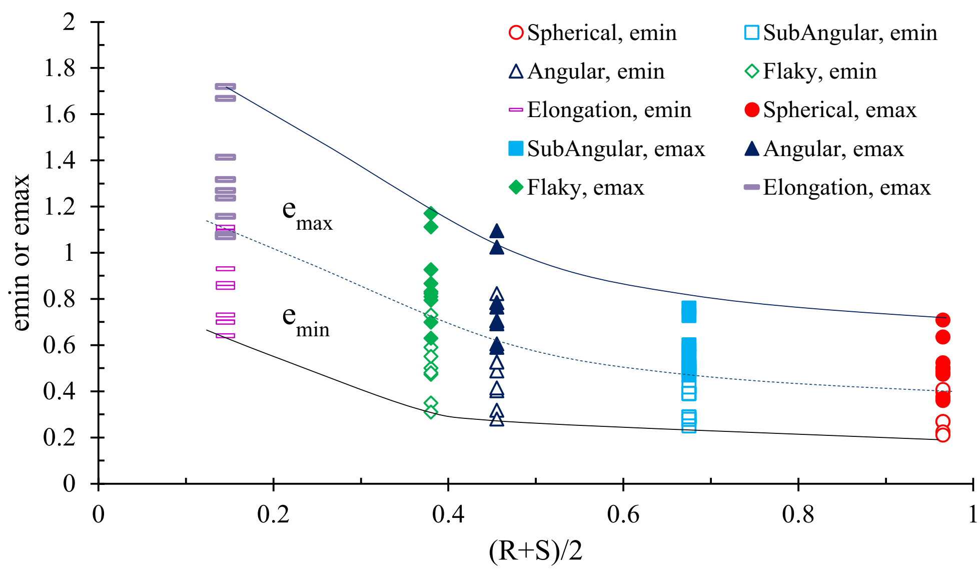

Fig. 5 Void ratio limits as a function of particle shape for samples with different *Cu*

4.2 Exploring a larger database

In addition to the current study tests, a database was collected from the literature, including 336 sands and glass beads (totally 381 tests). In this regard, the values of R, S, Cu, D_{50}, e_{max}, and e_{min} were documented and summarized in the Appendix Table. Generally, the roundness, R varied from 0.1 (for angular and elongated sand) to 1.0 (for glass spheres); the sphericity, S, ranged from 0.10 (flaky and elongated particles) to 1.0; the uniformity coefficient, Cu from 1.1 to 36.5, and the mean diameter, D_{50} from 0.07 to 3.79 mm.

First, the particle size (D_{50}), PSD curve (Cu), and particle shape (R, S, and ρ) were evaluated as single predictive variables for the limit void ratios.

The study revealed that D_{50} has no significant effect on the limit void ratios of sandy soils, which was also found previously by other researchers [8], [13], [17], [43]. As a result, the trends detected in the database analysis are attributable to the multivariable regression, including R, S, and Cu (see Figs. 6 and 7). Also, this model is normalized by the limit void ratios of the ideal mono-size spheres, e°_{max} and e°_{min}. The evolution of the minimum and maximum void ratios with respect to the regularity parameter, ρ, and Cu, including our experimental data and the dataset from the literature, are given in Figs. 6 and 7, respectively.

Predictive relationships for the limit void ratios were designed using a multivariable regression analysis through the database collected from the literature and the current experimental results.

$$e_{max} = R^{-0.32} S^{-0.2} C_u^{-0.2} e^{\circ}_{max},\ R^2 = 0.654 \quad (1)$$

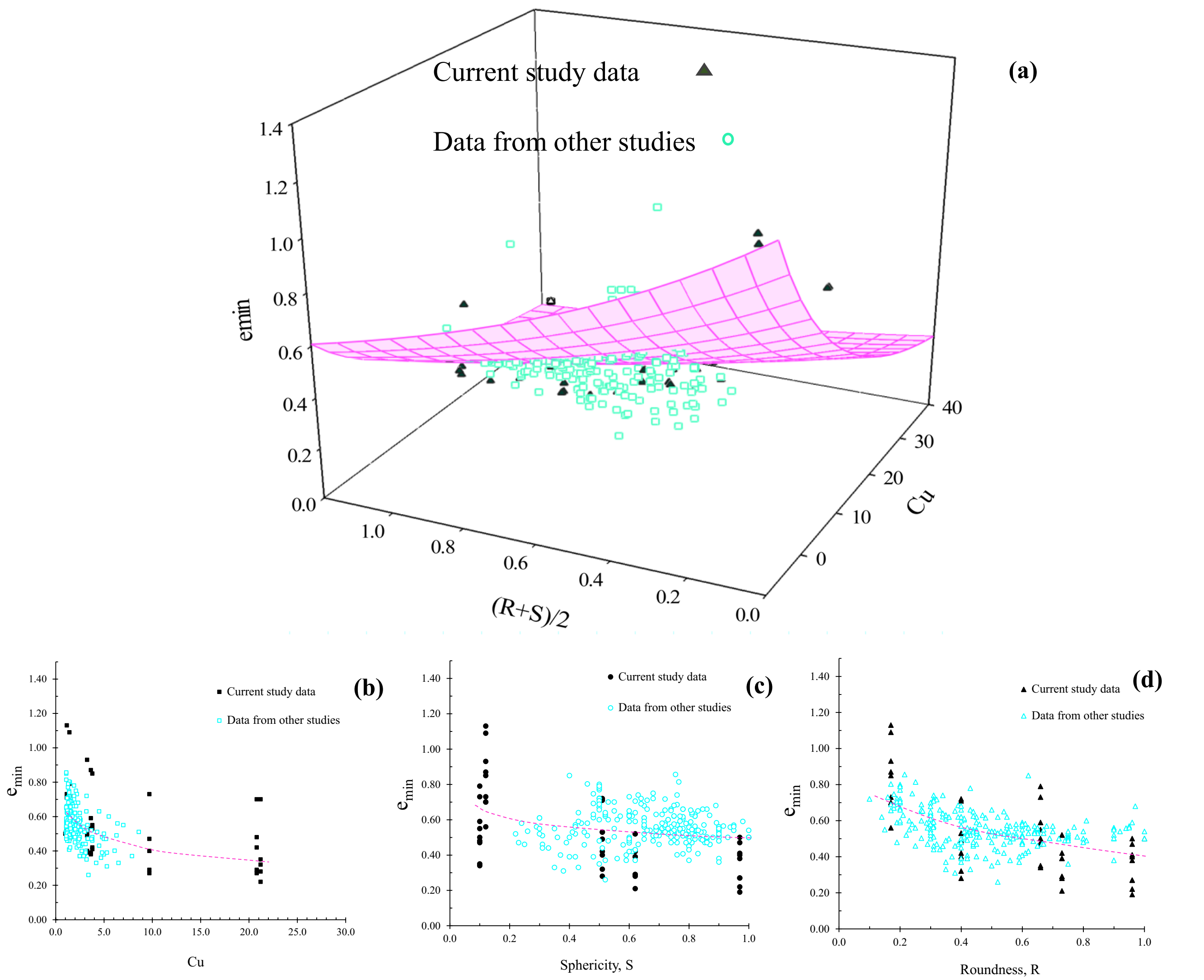

Fig. 6 **a**: Dependency of the minimum void ratio to the uniformity coefficient and the regularity parameter (database from other researchers and current study), **b**, **c**, and **d**: the minimum void ratio versus the uniformity coefficient (*Cu*), sphericity (*S*), and roundness (*R*), respectively

$$e_{min} = R^{-0.3} S^{-0.2} C_u^{-0.26} e^{\circ}_{min},\ R^2 = 0.623 \quad (2)$$

where e°_{max} and e°_{min} are the maximum and minimum void ratios for ideal mono-size spheres with $R = S = Cu = 1.0$, respectively. Where e°_{max} and e°_{min} are equal to 0.75 and 0.50, respectively [13].

The predicted and measured values of the limit void ratios by the current model were compared to the models developed by Chapuis [6], Zheng and Hryciw [13], and Sarkar et al. [43], based on experimental data belonging to this study on the glass sphere and sands, together with other data on similar materials reported by Sarkar et al. [43] and Zheng and Hryciw [13].

Statistical analyses, including the regression factor (R^2), the standard deviation (SD), and the mean absolute error or mean absolute difference (MAD) [52], were performed on the experimental results. Comparison between the results of the proposed predictive models and measured values for the minimum and maximum void ratios are given in Figs. 8 and 9, respectively.

The model proposed by Chapuis [6] obtained a MAD of 0.197 for both e_{max} and e_{min}. The model represented by Zheng and Hryciw [13] provided a MAD of 0.118 and 0.0584 for e_{max} and e_{min}, respectively, while the models developed by Sarkar et al. [43] led to a MAD of 0.0803 and 0.0524 for e_{max} and e_{min}, respectively.

The model proposed herein fairly fitted the overall test data. Moreover, the mean absolute deviation (MAD) between the observation and prediction were 0.0598 and 0.0394 for e_{min} and e_{max}, respectively. Then, the proposed model has the smallest MAD and the higher correlation

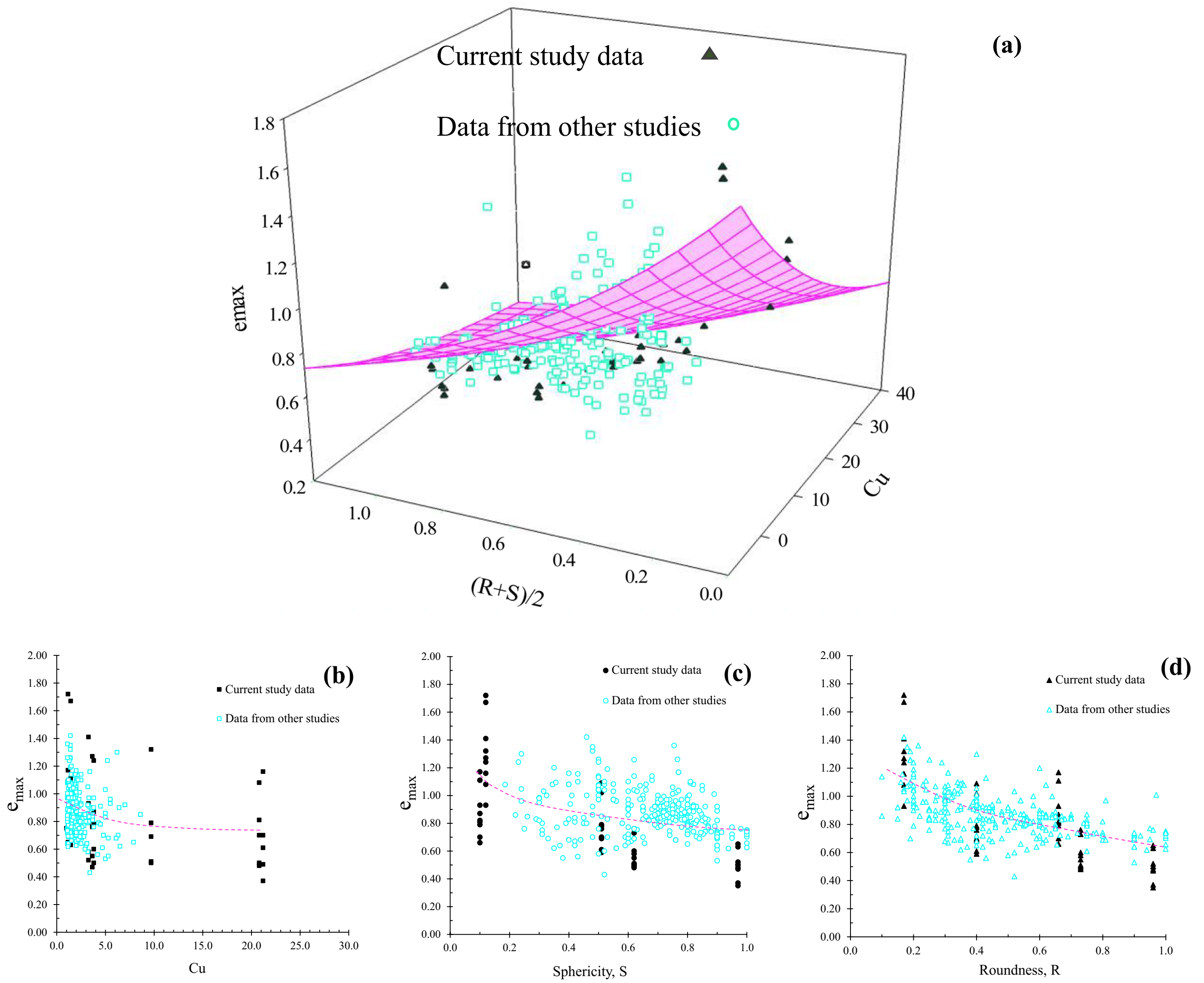

Fig. 7 **a**: Dependency of the maximum void ratio to the uniformity coefficient and the regularity parameter (database from other researchers and current study), **b**, **c**, and **d**: the maximum void ratio versus the uniformity coefficient (*Cu*), sphericity (*S*), and roundness (*R*), respectively

coefficient (R^2), which warranties a better estimate of the reference void ratios compared to previous models.

The maximum prediction error was observed in the packing model proposed by Chapuis [6], and this model generally underestimated the two limit void ratios. Indeed, the model just involves a dependency with *Cu* and roundness while the particle sphericity was ignored. Besides, the Chapuis [6] equations' provide a poor prediction for flaky particles' limit densities that have low sphericity in 3D space and a high roundness in 2D.

Zheng and Hryciw [13] considered sphericity in the particle projection area, and their predictive model has a maximum error in flaky particles. Furthermore, their model does not provide a proper prediction for elongated particles [13]. Finally, Sarkar et al. [43] model underestimate values when the particles have low sphericity and a low roundness (elongated particles). This issue may be due to the kind of sand particles involved in their experiments that generally were characterized with a medium to high sphericity. Moreover, their database did not involve particles with low sphericity.

The new predictive model shows a good agreement with both the experimental results obtained from the current study and the data used [13], [43]. Further, this new empirical model was developed over a large range of grain sizes and particle shapes.

4.3 Void ratio range

The difference between the limit void ratios gradually decreases while particle regularity increases (Fig. 5). Equations (1) and (2) reveal that ratio e_{max}/e_{min} is a function

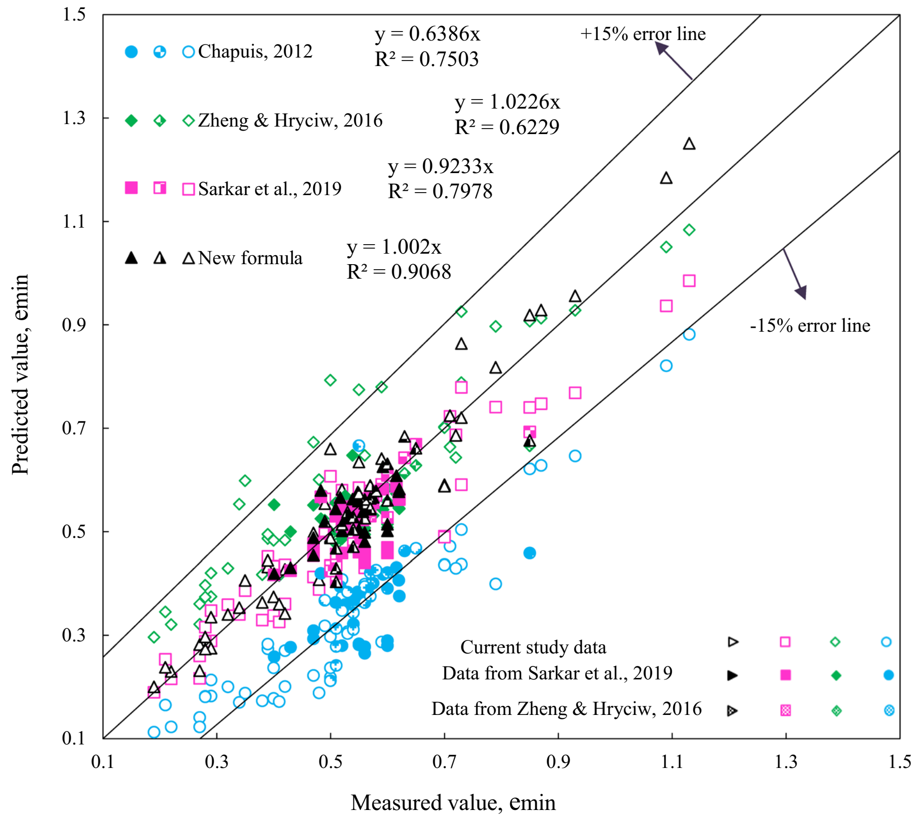

Fig. 8 Comparison between the proposed predictive equations and measured the minimum void ratio for experimental data from the current study, Sarkar et al. [43], and Zheng and Hryciw [13]

of *Cu*/*R*, as previously stated by [13]. Nevertheless, their relationships do not provide a good estimate for e_{max}/e_{min} ($R^2=0.138$), especially for irregular broadly graded materials, with higher *Cu*/*R*.

In this study, the relationships giving the limit void ratios involve an exponential function with regard to both *Cu* and ρ (Eq. 3, Table 6), which leads to a better prediction for e_{max}/e_{min} ($R^2=0.32$) than that when involving *Cu*/*R*.

Figure 10 illustrates the variation in maximum and minimum void ratios for the coefficient of uniformity and roundness.

This study also led to a linear relationship between e_{max} and e_{min} with $R^2=0.818$ (Eqs. 3 and 4, see Table 6).

5 Discussion

Unlike the previous investigations, the proposed equations are able to cover the extreme void properties of the particles with low sphericity such as flaky and elongated particles with fairly acceptable accuracy. However, some challenges must be considered.

The proposed equations are applicable for predicting the limit void ratios for a wide range of granular materials from sandy soils to rockfills. It should be noted that using the proposed equation in practical experiments might have some boundaries. This is due to the procedure of the ASTM that may not mimic packing and coalescence history in rockfill and mining applications and the size distribution steepness parameter *Cu* may not be well suited to capturing the size range in non-soil applications.

All considered soils were composed of a coarser and finer fraction inducing sometimes specific features. For example, in gap-graded and upward concave graded soils, the fine particles can move through the soil matrix due to vibration forces [53]. During the tests, the finer particle can move through the soil's skeleton void, without changing the total volume of the sample [16]. Further segregation may also occur during the test [54]. Accordingly, the developed models for predicting the limit void ratios should not be utilized for gap-graded soils [13]. Besides, for the upward concave graded soils, they should be used with some cautions.

The size distribution procedure in this research was performed using square-mesh sieves and the acquired gradation can be considered as a function of particle projection in two-dimensional assumption. So, the maximum width and thickness would be the governing criteria of the grading curve shape [16]. Thus, the grading curve shape would be changed, especially for flaky and elongated grains [48], [55]. Further, shape distribution might change in each shape class and the overall average shape indicator for particle assembly is better to be assumed. It must be noted that the chosen particles

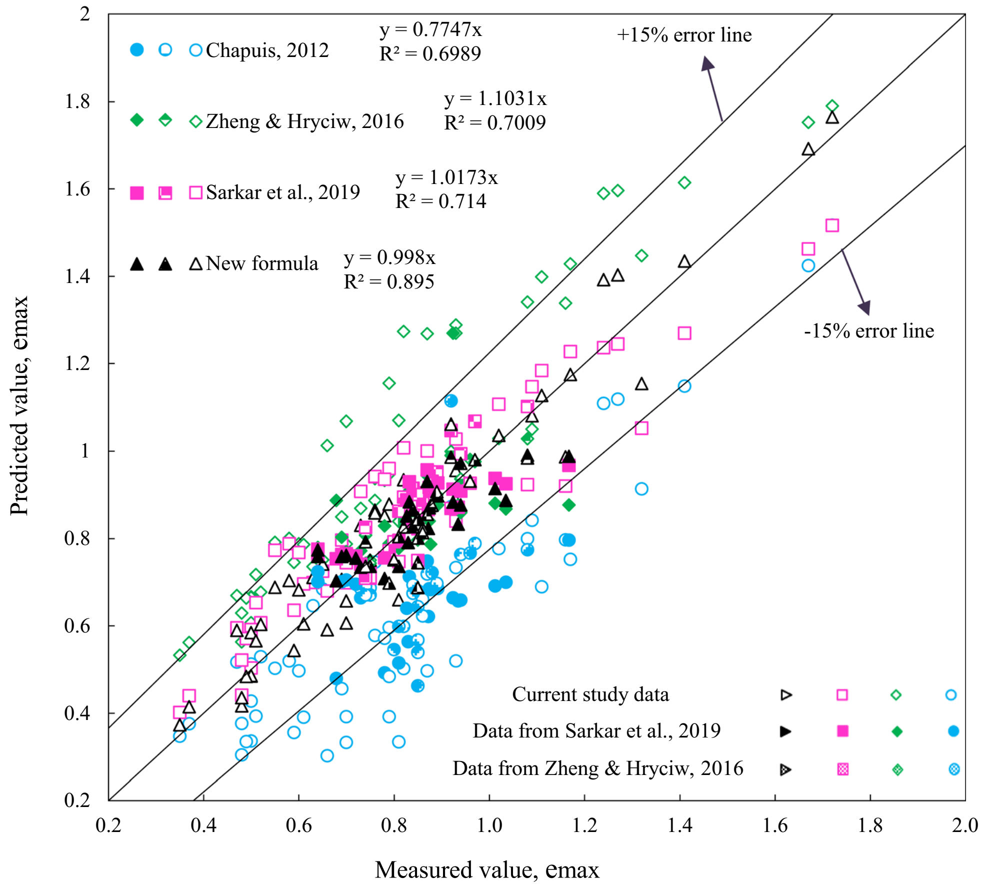

Fig. 9 Comparison between the proposed predictive equations and measured maximum void ratio for experimental data from the current study, Sarkar et al. [43], and Zheng and Hryciw [13]

Table 6 Relationships relating the limit void ratios one with each other

Predictive relationships	References
$e_{max} - e_{min} = (e^{\circ}_{max} - e^{\circ}_{min})(C_u^{-0.1} * \rho^{-0.45}$	(3) (all data, $R^2 = 0.32$)
$e_{max} = 1.382\ e_{min} + 0.104$	(4) (all data, $R^2 = 0.818$)
$e_{max} = 1.414\ e_{min} + 0.0795$	(5) (current study, $R^2 = 0.938$)

are ideal geometrical characteristics (i.e. spherical particles), identical geomorphologies (i.e. rounded, flaky and elongated particles), and manufactured aggregates (i.e. crushed grains) for which the shape feature of each class is assumed to be close to the overall values.

Although the results demonstrate general trends of reducing limit void ratios with increasing *R*, *S*, and *Cu* (Figs. 3, 4, 5, and 6), there is a large scatter in the data (Figs. 5 and 6). This may be attributed to both various particle shape classification and different procedures for determining the limit void ratios.

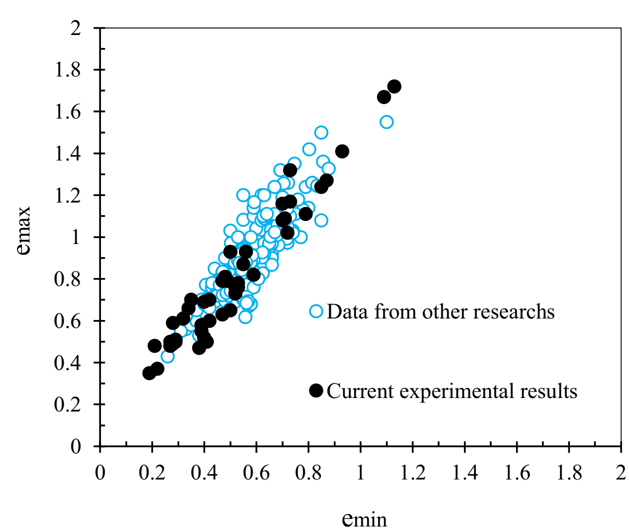

Fig. 10 Variation of maximum void ratio and minimum void ratio

In the lack of a standard method for particle shape classification, in practice, the particle shape is commonly described by qualitative visual comparison or quantified in projection planes [48]. Therefore, sphericity and/or roundness will be dissimilar in identical soils. Besides, variety in procedures to determine the limit void ratios, either in standard or non-standard methods, is supposed to induce a general scatter at the time when comparing different databases [2], [3].

A predictive model for the limit void ratios was designed based on the particles' regularity $(R+S)/2$. However, independent contributions of S and R in the limit void ratios may cause a bias in the predictions [43]. Nevertheless, particle regularity may be an appropriate index for rounded flaky particles with low sphericity in 3D space and a high roundness in 2D. It may be noted that gravity plays a different role in the packing of flaky particles than elongated particles because the center of mass finding lower energy states more easily in the former ones.

A model was formulated employing entire experimental database for the prediction of the limit void ratios involving particle regularity, ρ, and Cu (Eqs. 6 and 7). This predictive empirical model showed a good agreement with the measured experimental data (obtained from the current study but also the data from Sarkar et al. [43], and Zheng and Hryciw [13] as depicted in Figs. 11 and 12

$$e_{max} = \rho^{-0.48} C_u^{-0.21} e^{\circ}_{max}, \text{ All data}, R^2 = 0.629 \tag{6}$$

$$e_{min} = \rho^{-0.48} C_u^{-0.27} e^{\circ}_{min}, \text{ All data}, R^2 = 0.605 \tag{7}$$

6 Conclusions

This study aimed to evaluate the factors that control the limit void ratios of granular materials and the void ratio range on a series of glass beads and sands with various particle size distributions and particle shapes. The effect of the particle shapes is taken into account with nine identical gradations and in each case different particle shapes.

First, the influence of particle size (D_{50}), PSD curve (Cu), and particle shape (R, S, and ρ) on the limit void ratios were evaluated using current experimental results obtained by the authors. We found that the widely distributed grading soils have lower limit void ratios than poorly graded soils for the same grain shapes. Moreover, as the particles become more rounded and sphericity increases, the limit void ratios tend to decrease. Then, a database was created gathering experimental results documented in the literature. New multivariable empirical equations were developed to predict the limit void ratios and the void ratio range on the basis of this large database, and the prediction of the limit void ratios was

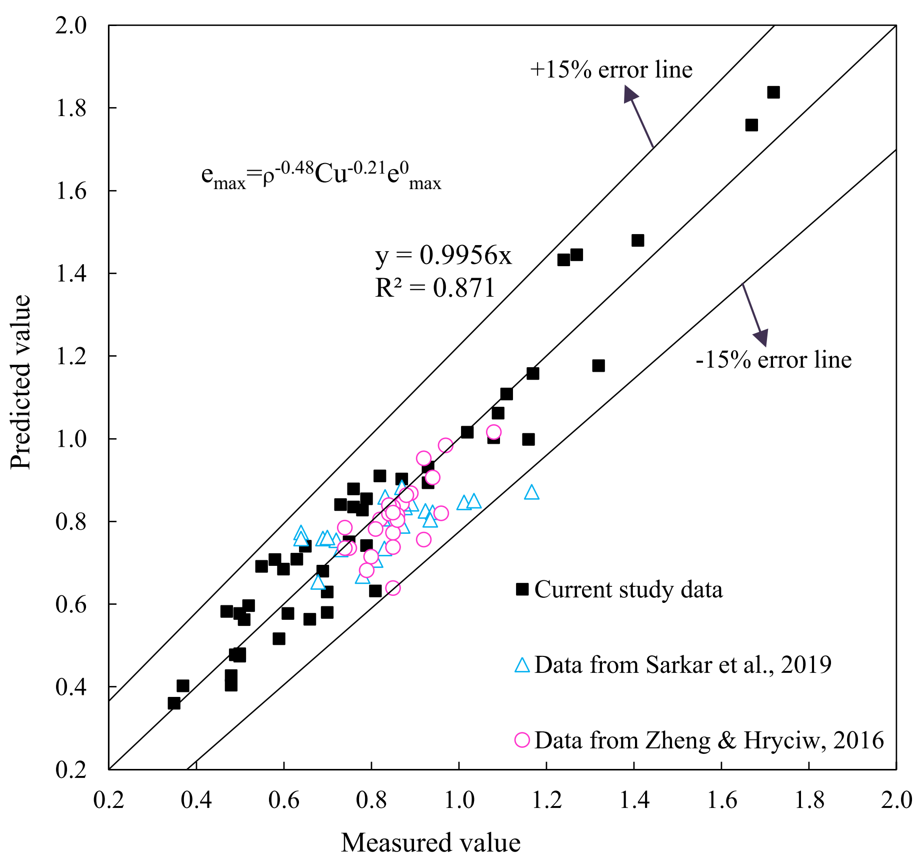

Fig. 11 The predicted and measured values of the maximum void ratio for experimental data from the current study, Sarkar et al. [43], and Zheng and Hryciw [13]

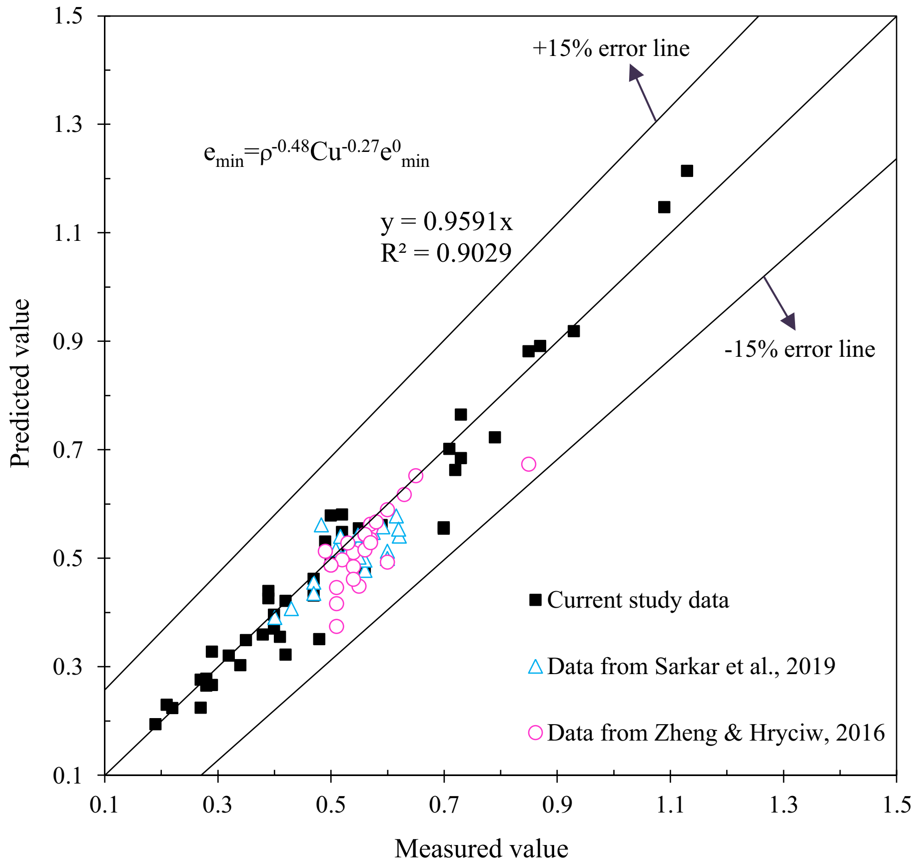

Fig. 12 The predicted and measured values of the minimum void ratio for experimental data from the current study, Sarkar et al. [43], and Zheng and Hryciw [13]

compared with the one obtained by using previous empirical formulas proposed by different authors.

The models proposed by the authors provide more accurate predictions for e_{max}, e_{min}, and e_{max}-e_{min} with a higher R^2 and a smaller MAD. Contrary to previous models, the proposed model can predict the limit void ratios for particles with low sphericity such as elongated and flaky particles with good accuracy.

Appendix

See Table 7

Table 7 …

References	*Cu*	D_{50}	*R*	*S*	e_{max}	e_{min}	Soil name/morphology
[57]	1.39		0.74	0.86	0.81	0.49	Bulky, spheroidal, rounded to well-rounded grains
	1.78		0.31	0.42	0.67	0.57	Flaky, oblate, angular grains composed of shells
	2.57		0.3	0.44	0.68	0.58	Flaky, oblate, angular grains
	4.81		0.19	0.53	0.7	0.48	Bulky, elongated, very angular grains coated with carbonate
[49]	1.27		0.2		1	0.77	Crushed
	1.58		0.18		0.97	0.67	Crushed
	1.7		0.17		1.05	0.69	Crushed
	1.74		0.2		0.97	0.67	Crushed
[13]b	1.06	0.74	0.78	0.9	0.74	0.51	Ottawa 20–30
	1.47	0.75	0.2	0.5	1.14	0.8	Q-Rok
[13]b	1.8	0.38	0.41	0.93	0.81	0.5	Sand O
	2	1.64	0.14	0.57	1.2	0.62	Sand L
[13]c	1.5	0.16	0.35	0.65	0.97	0.61	Toyoura sand
[13]a	2	0.28	0.55	0.75	0.94	0.62	Nerlerk[57]
	1.2	0.86	0.5	0.82	0.82	0.54	Leighton Buzzard
[8]	1.4		0.44		0.754	0.46	Lapis Lustre sand
	1.4		0.39		0.772	0.469	Monterey sand 1
	1.4		0.34		0.799	0.458	Monterey sand 2
	1.4		0.6		0.704	0.408	Ottawa sand 1
	1.4		0.42		0.772	0.407	Ottawa sand 2
	1.4		0.38		0.83	0.46	Ottawa sand 3
	1.4		0.27		0.971	0.503	Del Monte white sand 1
	1.4		0.23		1.082	0.55	Del Monte white sand 2
	1.4		0.21				Del Monte white sand 3
	1.4		0.2		1.19	0.7	Crushed basalt 1
	1.4		0.19		1.26	0.722	Crushed basalt 2
	1.4		0.19		1.32	0.692	Crushed basalt 3
	1.4		0.18		1.35	0.747	Crushed basalt 4
	1.4		0.17		1.42	0.803	Crushed basalt 5
	1.4		0.34		0.799	0.458	MOL
	2.5		0.35		0.688	0.37	MOL
	1.4		0.19		1.257	0.705	CB
	2.5	0.74	0.19		1.099	0.59	CB
[44]	≤2		0.165		1.156		Sand
	≤2		0.185		1.078		Sand
	≤2		0.24		1.047		Sand
	≤2		0.3		0.983		Sand
	≤2		0.325		1		Sand
	≤2		0.345		1.079		Sand
	≤2		0.356		1.094		Sand
	≤2		0.405		0.938		Sand
	≤2		0.315		1.031		Gravel
	≤2		0.3		0.983		Gravel
	≤2		0.655		0.656		Gravel
	≤2		1		0.703		Glass bead
	≤2		1		0.657		Glass bead
	≤2		1		0.625		Glass bead

Table 7 (continued)

References	Cu	D_{50}	R	S	e_{max}	e_{min}	Soil name/morphology
[58]	1.4	0.23	0.3	0.7	1	0.64	Daytona Beach sand
	1.9	0.3	0.43	0.5	1.13	0.78	Fraser River sand
	2.4	0.53	0.32	0.81	0.78	0.47	Ottawa #20/70 sand
	2.1	0.57	0.24	0.68	1.11	0.75	Ottawa #45 sand
	2.4	0.21	0.65	0.78	0.85	0.55	Ottawa #60/80 sand
	2.2	0.27	0.16	0.6	1.1	0.73	Ottawa #90 sand
	2.5	0.18	0.2	0.62	1.14	0.59	Syncrude Tailings
[10]a	0.15	1.8	0.6	0.85	0.85	0.57	Nevada sand
	0.58	1.5	0.4	0.8	0.99	0.57	Ticino sand
	0.49	1.9	0.7	0.7	0.87		Margaret River sand
	0.6	1.4	0.8	0.9	0.69		ASTM 20/30 sand
	0.18	1.8	0.3	0.85	1.07		Ponte Vedra sand
	0.38	3.3	0.2	0.7	0.97		8M8 crushed sand
	0.52	2.3	0.25	0.7	0.91		9C1 crushed sand
	0.17	1.7	0.3	0.85	1.04		Jekyll Island sand
	0.35	1.7	0.8	0.9	0.82	0.5	ASTM graded sand
	0.71	1.9	0.3	0.55	1.03	0.7	Blasting sand
	0.32	1.4	1	1	0.72	0.54	Glass beads
	0.09	6.2	0.4	0.24	1.3		Granite powder
	0.72	1.2	0.9	0.9	0.74	0.5	Ottawa #20/30 sand
	0.12	1.7	0.7	0.7	0.85	0.54	Ottawa F-110 sand
	0.3	3.2	0.2	0.8	0.79		7U7 crushed sand
	0.3	3.4	0.2	0.4	1.16		1K9 crushed sand
	0.48	5	0.1	0.6	0.86		2Z8 crushed sand
	0.4	3.6	0.3	0.9	0.89		5Z9 crushed sand
	0.33	3.8	0.2	0.8	0.97		6H1 crushed sand
	0.33	3.5	0.2	0.8	0.9		9F1 crushed sand
	0.27	2.2	0.2	0.7	0.95		3P3 crushed sand
	0.33	5.5	0.2	0.75	0.93		6A2 crushed sand
	0.32	3.5	0.15	0.7	0.84		5U1 crushed sand
	0.36	2.4	0.55	0.7	0.79	0.51	Sand boil sand
	0.25	2.9	0.25	0.8	0.83		1O2 crushed sand
	0.21	2.8	0.3	0.7	0.77		1O6 crushed sand
	0.25	3.3	0.25	0.8	0.91		6F5 crushed sand
	0.32	3.7	0.25	0.8	0.85		8B8 crushed sand
	0.26	3.2	0.25	0.8	0.85		3C7 crushed sand
	0.28	3.5	0.25	0.8	0.84		2L6 crushed sand
[11]d	1.3	0.87	0.81	0.84	0.69	0.49	Badger sand
[59]	5	0.45	0.3	0.6	1.03	0.5	Crushed glass
	5	0.45	0.44	0.76	0.83	0.47	Rhein sand
	5	0.45	0.9	0.9	0.53	0.38	Round glass
[13]c	1.4	0.47	0.3	0.62	1.04	0.64	Hoston sand
[13]c	1.3	0.76	0.75	0.8	0.8	0.51	Abraded Leighton Buzzard
[60]c	3.7	1	0.75	0.65	0.83	0.52	Narli
	2.5	1.4	0.45	0.61	0.93	0.62	Crushed stone sand
	3.3	0.86	0.65	0.72	0.8	0.55	Birecik
	6.3	0.72	0.35	0.65	0.7	0.49	Trakya

Table 7 (continued)

References	*Cu*	D_{50}	*R*	*S*	e_{max}	e_{min}	Soil name/morphology
[61]c	1.6	—	0.8	0.8	0.74	0.54	Bronze ballotini
	1.7	—	0.4	0.6	0.94	0.62	River Welland sand
	6.4	—	0.25	0.65	0.9	0.56	Crushed feldspar
[62]c	1.3	0.3	0.55	0.75	0.87	0.53	Ham River sand
	1.2	0.21	0.65	0.71	0.87	0.54	Fontainebleau sand
	1.3	0.3	0.75	0.7	0.87	0.53	M31 sand
	1.3	0.15	0.3	0.65	1	0.61	Longstone sand
[13]c	1.6	0.28	0.45	0.65	0.92	0.59	Ham River
[43]c	1.5	0.6	0.6	0.75	0.86	0.52	Hawaiian sand
[13]c	1.5	0.19	0.65	0.65	0.89	0.56	Mol sand
[43]a	1.2	0.72	0.65	0.87	0.78	0.46	Ottawa 20–30
	1.2	0.42	0.6	0.9	0.82	0.48	Ottawa 35–45
	1.2	0.25	0.52	0.9	0.89	0.53	Ottawa 50–70
	1.2	0.18	0.5	0.9	0.92	0.54	Ottawa 70–100
	1.2	0.12	0.5	0.9	0.92	0.54	Ottawa 100–140
	1.2	0.72	0.44	0.71	0.92	0.55	Evanston Beach 20–30
	1.2	0.42	0.43	0.73	0.9	0.52	Evanston Beach 35–45
	1.2	0.25	0.41	0.73	0.92	0.54	Evanston Beach 50–70
	1.2	0.18	0.42	0.72	0.93	0.53	Evanston Beach 70–100
	1.2	0.72	0.36	0.52	1.08	0.62	Franklin Falls 20–30
	1.2	0.42	0.35	0.52	1.04	0.63	Franklin Falls 35–45
	1.2	0.25	0.34	0.52	1.1	0.64	Franklin Falls 50–70
[43]c	1.2	0.75	0.75	0.9	0.72	0.51	Ottawa 20–30
	1.1	0.22	0.7	0.8	0.84	0.57	Ottawa 50–70
	1.9	0.13	0.6	0.6	0.9	0.59	Ottawa 100–200
	2.4	0.23	0.45	0.75	0.83	0.54	Douglas Lake sand
	2.5	0.34	0.6	0.8	0.72	0.48	Ackerman Lake sand
	1.3	0.25	0.2	0.5	1.24	0.79	Agsco 50–80
	4.7	0.6	0.75	0.9	0.61	0.36	Daedalus sand
[43]a	2.5	0.5	0.4	0.65	0.92	0.57	Teesta sand
	1.9	0.23	0.2	0.74	0.97	0.66	Meghna sand
	1.9	0.13	0.1	0.68	1.14	0.72	Jamuna sand
[43]b,f	1.4	32.5	0.27	0.74	0.899	0.652	Gabbro
	1.4	32.5	0.3	0.65	0.975	0.679	Greywacke
	1.4	32.5	0.31	0.63	1.031	0.74	Slate
	1.4	32.5	0.31	0.64	0.973	0.72	Greywacke
	1.4	32.5	0.32	0.72	0.992	0.717	Gabbro + Greywacke
	1.4	32.5	0.34	0.76	1.02	0.74	Rhyolite
	1.4	32.5	0.39	0.76	0.961	0.685	Dolelite
	1.4	32.5	0.43	0.71	0.839	0.551	River gravel
	1.4	32.5	0.58	0.74	0.744	0.525	Beach gravel
	1.4	32.5	0.38	0.72	0.922	0.654	Rounded C
	1.4	32.5	0.41	0.78	0.846	0.605	Rounded B
[42]c	4.5	0.78	0.35	0.6	0.91	0.63	Bushehr Port
	3.2	0.43	0.2	0.5	1.05	0.72	HormuzIsland
[13]c	1.6	0.3	0.62	0.7	0.87	0.53	M31 sand
	1.4	0.72	0.8	0.9	0.74	0.5	Ottawa sand
[13]c	1.8	0.3	0.75	0.8	0.79	0.5	Evanston Beach sand
	1.9	0.5	0.8	0.9	0.72	0.48	Density sand

Table 7 (continued)

References	Cu	D_{50}	R	S	e_{max}	e_{min}	Soil name/morphology
[13]c	1.5	0.21	0.45	0.75	0.9	0.51	Fontainebleau sand
[13]c	3.8	0.75	0.4	0.68	0.9	0.48	Clean sand
[13]a	2.2	0.38	0.61	—	0.67	0.42	P1-S2
	2.7	0.3	0.59	—	0.7	0.4	P1-S4
	2.6	0.44	0.62	—	0.76	0.43	P1-S5
	2.4	0.34	0.62	—	0.69	0.43	P1-S6
	1.9	0.31	0.5	—	0.76	0.48	P1-S1
	2.3	0.31	0.4	—	0.83	0.5	P1-S3
	2	0.29	0.42	—	0.81	0.52	P1-S7
	2.3	0.16	0.24	—	0.96	0.58	P2-S3
	2.5	0.54	0.59	—	0.64	0.37	P3-S3
	3	0.48	0.56	—	0.62	0.38	P3-S5
	2.1	0.29	0.36	—	0.77	0.5	P3-S6
	1.8	0.22	0.46	—	0.8	0.51	P3-S7
	1.9	0.3	0.31	—	0.8	0.51	P2-S1
	2.1	0.2	0.29	—	0.83	0.56	P2-S2
	5.3	0.32	0.4	—	0.68	0.39	P2-S4
	4.2	0.5	0.43	—	0.56	0.33	P2-S9
	2.3	0.2	0.31	—	0.75	0.46	P2-S10
	3.4	3.5	0.52	—	0.43	0.26	P2-S11
	3.2	0.63	0.5	—	0.58	0.35	P3-S1
	4.8	0.48	0.48	—	0.7	0.39	P3-S2
	2	0.58	0.42	—	0.84	0.56	P4-S1
	5.3	0.69	0.38	—	0.55	0.31	P5-S1
	2.8	0.64	0.33	—	0.69	0.44	P2-S5
	3.8	0.27	0.25	—	0.76	0.46	P2-S6
	3.2	0.15	0.22	—	0.86	0.52	P2-S7
	3.1	0.5	0.37	—	0.64	0.4	P2-S8
	3.1	0.42	0.42	—	0.64	0.39	P2-S12
	2.9	0.7	0.52	—	0.6	0.37	P3-S4
	2.9	0.48	0.31	—	0.72	0.44	P4-S2
	6.5	0.77	0.35	—	0.62	0.33	P4-S3
[63]c	1.6	0.2	0.3	—	0.95	0.55	Hochstetten sand
	1.7	0.35	0.3	—	0.98	0.61	Hostun RF sand
	1.9	0.4	0.45	—	0.84	0.53	Karlsruhe sand
	3.1	0.25	0.51	—	0.85	0.44	Lausitz sand
	1.5	0.16	0.3	—	0.98	0.61	Toyoura sand
	2.6	0.5	0.3	—	0.82	0.52	Zbraslav sand
[13]	1.3	0.26	0.64	0.76	0.87	0.57	Chesterton, Indiana dunes
	1.4	0.71	0.75	0.82	0.74	0.49	Ottawa 20–30
	2.3	0.5	0.53	0.67	0.82	0.54	Michigan 2NS
	2.2	0.32	0.57	0.73	0.81	0.52	New Madrid, Missouri
	1.5	0.3	0.62	0.72	0.85	0.56	Michigan dunes
	1.6	0.31	0.65	0.72	0.86	0.53	Oakland County, Michigan
	7	0.58	0.15	0.69	0.92	0.55	Michigan 30A
	1.6	1.8	0.3	0.69	0.92	0.63	Fused aluminum oxide
	1.5	0.33	0.4	0.73	0.94	0.6	Scotts Valley, California

Table 7 (continued)

References	*Cu*	D_{50}	*R*	*S*	e_{max}	e_{min}	Soil name/morphology
	2.8	0.6	0.51	0.69	0.85	0.54	Upper Peninsula, Michigan
	8.6	0.44	0.41	0.68	0.85	0.51	Fort Davis, Texas
	3	0.36	0.55	0.82	0.8	0.51	Rincon, New Mexico
	5.5	0.8	0.23	0.56	0.96	0.6	Crushed gabbro
	1.6	0.35	0.48	0.72	0.89	0.57	Capitola, California
	1.1	0.7	1	1	0.75	0.5	Small glass beads
	1.1	0.97	1	1	0.74	0.5	Large glass beads
	1.4	0.61	0.68	0.76	0.84	0.57	Brady, Texas
	1.9	0.21	0.62	0.69	0.86	0.56	Class IIA, Michigan
	4.3	0.74	0.6	0.69	0.79	0.51	Griffin, Indiana
	2.9	0.64	0.64	0.66	0.85	0.54	Chesterton, Indiana beach
	1.6	0.4	0.55	0.74	0.84	0.56	Muskegon, Michigan
	1.3	0.16	0.61	0.72	0.88	0.58	Nevada sand
	1.8	0.25	0.56	0.72	0.85	0.57	Treasure Island, California
	1.1	1.51	0.62	0.4	1.08	0.85	Long-grain rice
	1.1	1.91	0.54	0.55	0.97	0.65	Short-grain rice
[64]d	1.15	0.72	0.69	0.74	0.714	0.502	quartz sands
	1.43	0.26	0.41	0.48	0.861	0.612	quartz sands
	1.62	0.14	0.3	0.26	0.848	0.535	quartz sands
[65]	1.32	2.68	0.43	0.86	0.92	0.66	FS Ohio 6–10
	1.32	1.59	0.44	0.83	0.92	0.65	FS Ohio 10–16
	1.19	1.01	0.4	0.78	0.97	0.66	FS Ohio 16–20
	1.44	0.63	0.39	0.82	0.91	0.62	FS Ohio 20–40
	1.45	0.23	0.35	0.82	0.93	0.63	FS Ohio 50–100
	2	0.35	0.4	0.8	0.72	0.48	FS Ohio fine
	2	1.5	0.4	0.8	0.72	0.45	FS Ohio coarse
	7.9	1.04	0.4	0.8	0.65	0.37	FS Ohio SW
	–	0.62	0.43	0.83	0.81	0.59	Ohio Gold Frac
	1.19	0.72	0.72	0.88	0.74	0.5	Ottawa 20–30
[66]	1.70	0.66	0.67	0.85	0.85	0.53	Quartz sand
	1.67	0.34	0.67	0.73	0.86	0.55	Quartz sand
	2.14	0.1	0.58	0.79	0.82	0.51	Quartz sand
	1.75	0.27	0.81	0.73	0.97	0.6	Quartz sand
	2.32	0.12	0.97	0.89	1.01	0.68	Quartz sand with silt and clay
[43]	2	0.25	0.44	0.77	0.924	0.539	Rhein sand
	2	0.25	0.4	0.75	1.012	0.621	Hostun sand
	2	0.25	0.49	0.78	0.827	0.509	Siligram sand
	2	0.25	0.45	0.77	0.94	0.549	Silbersand + black sand
	2	0.25	0.31	0.77	1.167	0.592	Greywacke
	1.33	1.5	0.48	0.78	0.87	0.616	Sackware 1–2 mm
	2.03	0.53	0.54	0.78	0.872	0.526	Sackware 0.2–1 mm
	1.38	0.17	0.56	0.75	0.832	0.483	Cardiff sand
	1.78	0.22	0.45	0.77	0.892	0.548	Silbersand

Table 7 (continued)

References	Cu	D_{50}	R	S	e_{max}	e_{min}	Soil name/morphology
	6.1	0.85	0.45	0.76	0.679	0.401	Black sand
	1.62	0.19	0.51	0.79	0.877	0.517	Norm sand
	1.5	0.17	0.52	0.77	1.035	0.62	Sackware fs S90
	1.68	0.3	0.58	0.8	0.935	0.557	Sackware 0.1–0.5 mm
	1.54	0.74	0.55	0.75	0.874	0.575	Sackware 0.5–1 mm
	3.3	0.4	0.45	0.79	0.83	0.47	Mix sand (sand 1)
	4.5	0.75	0.52	0.8	0.78	0.43	Mix sand (sand 2)
	3.7	0.5	0.54	0.74	0.81	0.47	Mix sand (sand 3)
	1.21	0.17	0.9	0.9	0.69	0.52	Glass beads-1
	1.43	0.38	0.9	0.9	0.73	0.56	Glass beads-2
	1.24	0.5	0.9	0.9	0.72	0.56	Glass beads-3
	1.19	0.61	0.9	0.9	0.7	0.55	Glass beads-4
	1.1	1.4	0.9	0.9			Glass beads-5
	1.21	5.5	0.9	0.9			Glass beads-6
[67]	1.12	0.68	0.72	0.86	0.74	0.5	Ottawa 20–30
	1.86	0.36	0.57	0.76	0.82	0.5	ASTM graded
	1.49	0.25	0.47	0.71	0.97	0.63	Toyoura
	1.26	1.07	0.31	0.66	1.08	0.71	K4
	1.59	0.76	0.27	0.64	1.07	0.69	K5
	1.56	0.43	0.33	0.66	1.04	0.66	K6
	1.1	0.95	0.92	0.95	0.72	0.54	Glass beads
[68]	1.19	0.72	0.9	0.86	0.74	0.502	Ottawa 20/30
	1.55	0.217	0.75	0.83	0.81	0.54	Ottawa F-75
	1.19	1.01	0.2		1.077	0.707	crushed sands K-4
	1.47	0.798	0.18		1.071	0.688	crushed sands K-5
	1.52	0.467	0.17		1.035	0.656	crushed sands K-6
	1.7	0.163	0.2		1.041	0.6	crushed sands K-7
[69]d	2.12	0.236	0.5	0.78	0.9	0.66	beach sand, Type 1
	1.5	0.316	0.46	0.71	0.78	0.58	beach/ alluvial sand, Type 5
	1.73	0.235	0.27	0.53	0.83	0.6	beach sand, Type 9
	3.18	0.369	0.21	0.48	0.92	0.63	alluvial sand, Type 13
[70]d			0.3	0.63	0.92	0.65	Bucarest
			0.21	0.41	1.18	0.85	Calcare
			0.41	0.47	1.11	0.81	Colleferro
			0.14	0.23	1.31	0.87	Fumone
			0.35	0.54	1.13	0.71	Milano
			0.48	0.75	1.01	0.69	Roma
			0.65	0.86	0.92	0.64	Torre del
[71][d	1.16	0.7	0.94	0.938	0.618	0.558	Rounded glass beads
	1.16	0.7	0.77	0.915	0.735	0.564	A25R75
	1.16	0.7	0.61	0.892	0.778	0.583	A50R50
	1.16	0.7	0.44	0.869	0.827	0.625	A75R25
	1.16	0.7	0.27	0.846	0.867	0.66	Angular glass beads

Table 7 (continued)

References	Cu	D_{50}	R	S	e_{max}	e_{min}	Soil name/morphology
[41]	1.5	3.082	0.54		0.661	0.42	Plymouth Beach sand
	1.5	1.304	0.44		0.693	0.481	Plymouth Beach sand
	1.4	0.601	0.42		0.72	0.492	Plymouth Beach sand
	1.3	0.326	0.34		0.902	0.622	Plymouth Beach sand
	1.2	0.212	0.3		0.97	0.65	Plymouth Beach sand
[41]	1.2	0.714	0.36	0.82	1.08	0.62	Franklin Falls sand
	1.2	0.421	0.35	0.81	1.09	0.63	Franklin Falls sand
	1.2	0.252	0.34	0.81	1.1	0.64	Franklin Falls sand
	1.2	0.714	0.65	0.87	0.77	0.46	Ottawa sand
	1.2	0.421	0.6	0.85	0.82	0.48	Ottawa sand
	1.2	0.252	0.52	0.84	0.89	0.53	Ottawa sand
	1.2	0.178	0.5	0.83	0.92	0.54	Ottawa sand
	1.2	0.126	0.5	0.82	0.92	0.54	Ottawa sand
[41]	1.1	0.922	0.665	0.853	0.723	0.471	Diagenetic sand
	1.1	0.324	0.636	0.845	0.733	0.486	Diagenetic sand
	1.1	0.115	0.556	0.826	0.799	0.539	Diagenetic sand
	1.1	2.571	0.491	0.831	0.82	0.54	Felton Beach sand
	1.1	0.922	0.309	0.82	0.884	0.563	Felton Beach sand
	1.1	0.324	0.274	0.806	1.002	0.654	Felton Beach sand
	1.1	0.115	0.215	0.755	1.36	0.856	Felton Beach sand
	1.1	2.571	0.451	0.81	0.843	0.544	Bear Riversand
	1.1	0.922	0.287	0.806	0.888	0.588	Bear River sand
	1.1	0.115	0.251	0.766	1.26	0.814	Bear River sand
[72]	1.3	0.31	0.4	0.75	1.059	0.681	Hostun sand (D1)
	1.3	0.67	0.6	0.79	0.879	0.579	Quartz sand (0.5–1 mm) (D2)
	3.3	0.45	0.67	0.86	0.834	0.471	Sand mixture (D3)
	1.2	1.36	0.95	0.95	0.693	0.569	Round glass beads (1.25–1.55 mm) (D4)
	1.2	0.05	0.95	0.95	0.772	0.561	Round glass beads powder (d1)
	5.8	0.025	0.6	0.7	1.619	1.059	Split (d2)
	4.1	0.027	0.55	0.75	1.725	1.037	Silt (Schluff) (d3)
	5.8	0.024	0.3	0.6	1.911	1.19	Crushed glass beads powder (d4)
[73]	1.55	0.223	0.64	0.41	1	0.53	Babolsar sand
	1.51	0.218	0.6	0.35	1.2	0.55	Qare-Aqaj sand
	2.42	0.387	0.6	0.39	0.8	0.47	Bushehr sand
	1.47	0.276	0.58	0.46	1	0.58	Clean Firoozkuh sand
	1.49	0.276	0.96	0.98	0.76	0.59	Glass beads
	5.22	0.166	0.29	0.23	1.24	0.47	Golgohar tailings
Current study	1.16	0.22	0.96	0.97	0.65	0.50	Glass bead
	1.16	0.22	0.73	0.62	0.76	0.52	Firozkooh rounded sand
	1.16	0.22	0.4	0.51	1.09	0.71	Crushed aggregate
	1.16	0.22	0.66	0.1	1.17	0.73	Flaky slate
	1.16	0.22	0.17	0.12	1.72	1.13	Pyramid basalt
	1.43	3.52	0.96	0.97	0.63	0.47	Glass bead
	1.43	3.52	0.73	0.62	0.73	0.52	Firozkooh rounded sand
	1.43	3.52	0.4	0.51	1.02	0.72	Crushed aggregate
	1.43	3.52	0.66	0.1	1.11	0.79	Flaky slate
	1.43	3.52	0.17	0.12	1.67	1.09	Pyramid basalt

Table 7 (continued)

References	Cu	D_{50}	R	S	e_{max}	e_{min}	Soil name/morphology
	3.65	3.05	0.96	0.97	0.52	0.40	Glass bead
	3.65	3.05	0.73	0.62	0.58	0.39	Firozkooh rounded sand
	3.65	3.05	0.4	0.51	0.79	0.49	Crushed aggregate
	3.65	3.05	0.66	0.1	0.93	0.50	Flaky slate
	3.65	3.05	0.17	0.12	1.41	1.03	Pyramid basalt
	3.26	3.05	0.96	0.97	0.47	0.38	Glass bead
	3.26	3.05	0.73	0.62	0.55	0.39	Firozkooh rounded sand
	3.26	3.05	0.4	0.51	0.76	0.53	Crushed aggregate
	3.26	3.05	0.66	0.1	0.82	0.59	Flaky slate
	3.26	3.05	0.17	0.12	1.13	0.77	Pyramid basalt
	3.8	3.54	0.96	0.97	0.50	0.41	Glass bead
	3.8	3.54	0.73	0.62	0.60	0.42	Firozkooh rounded sand
	3.8	3.54	0.4	0.51	0.78	0.53	Crushed aggregate
	3.8	3.54	0.66	0.1	0.87	0.55	Flaky slate
	3.8	3.54	0.17	0.12	1.24	0.85	Pyramid basalt
	9.7	3.79	0.96	0.97	0.50	0.27	Glass bead
	9.7	3.79	0.73	0.62	0.51	0.29	Firozkooh rounded sand
	9.7	3.79	0.4	0.51	0.69	0.40	Crushed aggregate
	9.7	3.79	0.66	0.1	0.79	0.47	Flaky slate
	9.7	3.79	0.17	0.12	1.32	0.73	Pyramid basalt
	20.8	3.67	0.96	0.97	0.48	0.27	Glass bead
	20.8	3.67	0.73	0.62	0.50	0.29	Firozkooh rounded sand
	20.8	3.67	0.4	0.51	0.70	0.42	Crushed aggregate
	20.8	3.67	0.66	0.1	0.81	0.48	Flaky slate
	20.8	3.67	0.17	0.12	1.28	0.70	Pyramid basalt
	21.2	2.85	0.96	0.97	0.37	0.22	Glass bead
	21.2	2.85	0.73	0.62	0.49	0.28	Firozkooh rounded sand
	21.2	2.85	0.4	0.51	0.61	0.32	Crushed aggregate
	21.2	2.85	0.66	0.1	0.70	0.35	Flaky slate
	21.2	2.85	0.17	0.12	1.16	0.70	Pyramid basalt
	36.5	2.34	0.96	0.97	0.35	0.19	Glass bead
	36.5	2.34	0.73	0.62	0.48	0.21	Firozkooh rounded sand
	36.5	2.34	0.4	0.51	0.59	0.28	Crushed aggregate
	36.5	2.34	0.66	0.1	0.66	0.34	Flaky slate
	36.5	2.34	0.17	0.12	0.93	0.56	Pyramid basalt

(a)Roundness and sphericity were estimated by visual comparison with standard charts developed by Krumbein and Sloss [74] or Krumbein [28], after [13]

(b)Roundness and sphericity were computed by Wadell's manual procedure, after [13]

(c)Roundness and sphericity are estimated based on written descriptions or particle images given in the reference, after [13]

(d)Roundness and sphericity are estimated based on visual comparison with charts suggested by [25]

References

1. Holubec, I., D'Appolonia, E.: Effect of particle shape on the engineering properties of granular soils. In: Evaluation of Relative Density and its Role in Geotechnical Projects Involving Cohesionless Soils. pp. 304–315. ASTM International, West Conshohocken, (1973)
2. Lade, P.V., Liggio, C.D., Yamamuro, J.A.: Effects of non-plastic fines on minimum and maximum void ratios of sand. Geotech. Test. J. **21**, 336–347 (1998). https://doi.org/10.1520/GTJ11373J
3. Yilmaz, Y.: A study on the limit void ratio characteristics of medium to fine mixed graded sands. Eng. Geol. **104**, 290–294 (2009). https://doi.org/10.1016/j.enggeo.2008.11.009
4. Maroof, M.A., Mahboubi, A., Noorzad, A.: Effects of grain morphology on suffusion susceptibility of cohesionless soils. Granul. Matter. **23**, 8 (2021). https://doi.org/10.1007/s10035-020-01075-1
5. Abbireddy, C.O.R., Clayton, C.R.I.: The impact of particle form on the packing and shear behaviour of some granular materials: an experimental study. Granul. Matter. **17**, 427–438 (2015). https://doi.org/10.1007/s10035-015-0566-0
6. Chapuis, R.P.: Estimating the in situ porosity of sandy soils sampled in boreholes. Eng. Geol. **141–142**, 57–64 (2012). https://doi.org/10.1016/j.enggeo.2012.04.015
7. Murphy, K.A., MacKeith, A.K., Roth, L.K., Jaeger, H.M.: The intertwined roles of particle shape and surface roughness in controlling the shear strength of a granular material. Granul. Matter. **21**, 1–6 (2019). https://doi.org/10.1007/s10035-019-0913-7
8. Youd, T.L.: Factors controlling maximum and minimum densities of sands. In: Evaluation of relative density and its role in geotechnical projects involving cohesionless soils, ASTM STP 525. pp. 98–112 (1973)
9. Miura, K., Maeda, K., Furukawa, M., Toki, S.: Mechanical characteristics of sands with different primary properties. Soils Found. **38**, 159–172 (1998). https://doi.org/10.1248/cpb.37.3229
10. Cho, G.-C., Dodds, J., Santamarina, J.C.: Particle shape effects on packing density, stiffness, and strength: natural and crushed sands. J. Geotech. Geoenviron. Eng. **132**, 591–602 (2006). https://doi.org/10.1061/(ASCE)1090-0241(2006)132:5(591)
11. Rousé, P.C., Fannin, R.J., Shuttle, D.A.: Influence of roundness on the void ratio and strength of uniform sand. Géotechnique. **58**, 227–231 (2008). https://doi.org/10.1680/geot.2008.58.3.227
12. Yilmaz, Y., Mollamahmutoglu, M.: Characterization of liquefaction susceptibility of sands by means of extreme void ratios and/or void ratio range. J. Geotech. Geoenviron. Eng. **135**, 1986–1990 (2009). https://doi.org/10.1061/(ASCE)GT.1943-5606.0000164
13. Zheng, J., Hryciw, R.D.: Index void ratios of sands from their intrinsic properties. J. Geotech. Geoenviron. Eng. **142**, 06016019 (2016). https://doi.org/10.1061/(ASCE)GT.1943-5606.0001575
14. Guises, R., Xiang, J., Latham, J.P., Munjiza, A.: Granular packing: Numerical simulation and the characterisation of the effect of particle shape. Granul. Matter. **11**, 281–292 (2009). https://doi.org/10.1007/s10035-009-0148-0
15. Cubrinovski, M., Ishihara, K.: Maximum and Minimum Void Ratio Characteristics of Sands. Soils Found. **42**, 65–78 (2002). https://doi.org/10.3208/sandf.42.6_65
16. Kezdi, A.: Soil Physics- Selected Topics. Elsevier, Amsterdam (1979)
17. Kovács, G.: Seepage hydraulics, Amsterdam (1981)
18. Aberg, B.: Grain-size distribution for smallest possible void ratio. J. Geotech. Eng. **122**, 74–77 (1996). https://doi.org/10.1061/(ASCE)0733-9410(1996)122:1(74)
19. Latham, J.P., Munjiza, A., Lu, Y.: On the prediction of void porosity and packing of rock particulates. Powder Technol. **125**, 10–27 (2002). https://doi.org/10.1016/S0032-5910(01)00493-4
20. Chang, C.S., Deng, Y., Yang, Z.: Modeling of minimum void ratio for granular soil with effect of particle size distribution. J. Eng. Mech. **143**, 04017060 (2017). https://doi.org/10.1061/(ASCE)EM.1943-7889.0001270
21. Riquelme, J., Dorador, L.: Methodology to determine maximum and minimum void index in coarse granular soils from small-scale tests correlations. In 70 th Canadian Geotechnical Conference In: Geoottawa, pp. 1–6 (2017)
22. Stringer, M.E., Cerna-Alvarez, E., Kutter, B.L.: Effects of the ratio between body forces and inter-particle forces on maximum void ratio. Soils Found. **60**, 1–12 (2020). https://doi.org/10.1016/j.sandf.2019.12.012
23. Barrett, P.J.: The shape of rock particles, a critical review. Sedimentology **27**, 291–303 (1980). https://doi.org/10.1111/j.1365-3091.1980.tb01179.x
24. Mitchell, J., Soga, K.: Fundamentals of soil behavior. Wiley, New York (2005)
25. Maroof, M.A., Mahboubi, A., Noorzad, A., Safi, Y.: A new approach to particle shape classification of granular materials. Transp. Geotech. **22**, 100296 (2020). https://doi.org/10.1016/j.trgeo.2019.100296
26. Wadell, H.: Sphericity and roundness of rock particles. J. Geol. **41**, 310–331 (1933). https://doi.org/10.1086/624040
27. Wentworth, C.K.: The shapes of rock particles: a discussion. J. Geol. **41**, 306–309 (1933). https://doi.org/10.3133/pp131C
28. Krumbein, W.C.: Measurement and geological significance of shape and roundness of sedimentary particles. J. Sediment. Res. **11**, 64–72 (1941). https://doi.org/10.1306/D42690F3-2B26-11D7-8648000102C1865D
29. Wadell, H.: Volume, shape, and roundness of rock particles. J. Geol. **40**, 443–451 (1932). https://doi.org/10.1086/623964
30. Powers, M.C.: A new roundness scale for sedimentary particles. SEPM J. Sediment. Res. **23**, 117–119 (1953). https://doi.org/10.1306/D4269567-2B26-11D7-8648000102C1865D
31. Deng, X.L., Davé, R.N.: Dynamic simulation of particle packing influenced by size, aspect ratio and surface energy. Granul. Matter. **15**, 401–415 (2013). https://doi.org/10.1007/s10035-013-0413-0
32. Seblany, F., Homberg, U., Vincens, E., Winkler, P., Josef Witt, K.: Merging criteria for defining pores and constrictions in numerical packing of spheres. Granul. Matter. **20**, 37 (2018). https://doi.org/10.1007/s10035-018-0808-z
33. Latham, J.-P., Xiang, J., Farsi, A., Joulin, C., Karantzoulis, N.: A class of particulate problems suited to FDEM requiring accurate simulation of shape effects in packed granular structures. Comput. Part. Mech. **7**, 975–986 (2020). https://doi.org/10.1007/s40571-019-00294-5
34. Farsi, A., Xiang, J., Latham, J.-P., Carlsson, M., Stitt, H., Marigo, M.: Packing simulations of complex-shaped rigid particles using FDEM: An application to catalyst pellets. Powder Technol. **380**, 443–461 (2021). https://doi.org/10.1016/j.powtec.2020.11.010
35. ASTM D4253–00: Standard test methods for maximum index density and unit weight of soils using a vibratory table. West Conshohocken, PA (2006)
36. Tsirel, S.V.: Methods of granular and fragmented material packing density calculation. Int. J. Rock Mech. Min. Sci. **34**, 263–273 (1997). https://doi.org/10.1016/S0148-9062(96)00029-0
37. Fuller, W., Thomson, S.: The laws of proportioning concrete. Trans. Am. Soc. Civ. Eng. LIX **59**, 67–143 (1907)
38. Peronius, N., Sweeting, T.J.: On the correlation of minimum porosity with particle size distribution. Powder Technol. **42**, 113–121 (1985). https://doi.org/10.1016/0032-5910(85)80043-7
39. Koerner, R.M.: Limiting density behavior of quartz powders. Powder Technol. **3**, 208–212 (1969). https://doi.org/10.1016/0032-5910(69)80079-3

40. GHafghazi, M., Azhari, F.: A simple method for estimating the non-structural fines content of granular materials. Icse, 6: 535–542 (2012)
41. Chang, C.S., Deng, Y., Meidani, M.: A multi-variable equation for relationship between limiting void ratios of uniform sands and morphological characteristics of their particles. Eng. Geol. **237**, 21–31 (2018). https://doi.org/10.1016/j.enggeo.2018.02.003
42. Hryciw, R.D., Zheng, J., Penn, R.: An Update of Robert M. Koerner's Models for the packing densities of sands using image-based intrinsic soil properties. In: Geo-Chicago. pp. 83–94 (2016)
43. Sarkar, D., König, D., Goudarzy, M.: The influence of particle characteristics on the index void ratios in granular materials. Particuology. (2019). https://doi.org/10.1016/j.partic.2018.09.010
44. Santamarina, J.C., Cho, G.C.: Soil behaviour: the role of particle shape. In: Skempton Conference. pp. 1–14. , London (2004)
45. Shen, C., Liu, S., Xu, S., Wang, L.: Rapid estimation of maximum and minimum void ratios of granular soils. Acta Geotech. **14**, 991–1001 (2019). https://doi.org/10.1007/s11440-018-0714-x
46. Cybermed Inc.: Operating manual, OnDemand3D application, (2015)
47. 3Dim Laboratory s.r.o.: 3DimViewer 3.1.1, (2017)
48. Maroof, M.A., Mahboubi, A., Noorzad, A.: A new method to determine specific surface area and shape coefficient of a cohesionless granular medium. Adv. Powder Technol. **31**, 3038–3049 (2020). https://doi.org/10.1016/j.apt.2020.05.028
49. Choo, H., Lim, S., Lee, W.: Determination of minimum void ratio of crushed rock sand using a vibrating table test. Geotech. Test. J. **41**, 20170167 (2018). https://doi.org/10.1520/GTJ20170167
50. Prochaska, A.B., Drnevich, V.P.: One-point vibrating hammer compaction test for granular soils. Adv Pavement Eng (2005). https://doi.org/10.1061/40776(155)6
51. ASTM D4254–00: Standard test methods for minimum index density and unit weight of soils and calculation of relative density., West Conshohocken, PA (2006)
52. Rezazadeh Eidgahee, D., Haddad, A., Naderpour, H.: Evaluation of shear strength parameters of granulated waste rubber using artificial neural networks and group method of data handling. Sci. Iran. **26**, 3233–3244 (2018).https://doi.org/10.24200/sci.2018.5663.1408
53. Kenney, T.C., Lau, D.: Internal stability of granular filters. Can. Geotech. J. **22**, 215–225 (1985). https://doi.org/10.1139/t86-068
54. USACE: US Army Corps of Engineers EM 1110–2–1911: Construction control for earth and rock-fill dams, Washington, D.C (1995)
55. Allen, T.: Particle size measurement. Springer, US, Boston, MA (1981)
56. Shimobe, S. Moroto, N.: A new classification chart for sand liquefaction. In: 1st, Earthquake geotechnical engineering. p. 6., Tokyo (1995)
57. Knodel, P., Yudhbir, A.R.: Quantification of particle shape and angularity using the image analyzer. Geotech. Test. J. **14**, 296 (1991). https://doi.org/10.1520/GTJ10574J
58. Sukumaran, B., Ashmawy, A.K.: Quantitative characterisation of the geometry of discret particles. Géotechnique. **51**, 619–627 (2001). https://doi.org/10.1680/geot.2001.51.7.619
59. Sarkar, D., Goudarzy, M., König, D.: An interpretation of the influence of particle shape on the mechanical behavior of granular material. Granul. Matter. **21**, 53 (2019). https://doi.org/10.1007/s10035-019-0909-3
60. Akbulut, A.F.C.N.: Effects of particle shape and size distributions on the hydraulic conductivity. Acta Geotech. Slov. **2**, 83–93 (2016)
61. Barden, L., Ismail, H., Tong, P.: Plane strain deformation of granular material at low and high pressures. Géotechnique. **19**, 441–452 (1969). https://doi.org/10.1680/geot.1969.19.4.441
62. Tsomokos, A., Georgiannou, V.N.: Effect of grain shape and angularity on the undrained response of fine sands. Can. Geotech. J. **47**, 539–551 (2010). https://doi.org/10.1139/T09-121
63. Herle, I., Gudehus, G.: Determination of parameters of a hypoplastic constitutive model from properties of grain assemblies. Mech. Cohesive-frictional Mater. **4**, 461–486 (1999). https://doi.org/10.1002/(SICI)1099-1484(199909)4:5<461::AID-CFM71>3.0.CO;2-P
64. Fuggle, A.R., Roozbahani, M.M., Frost, J.D.: Size effects on the void ratio of loosely packed binary particle mixtures. In: Geo-Congress 2014 Technical Papers. pp. 129–138. American Society of Civil Engineers, Reston, VA (2014)
65. Han, F., Ganju, E., Salgado, R., Prezzi, M.: Effects of interface roughness, particle geometry, and gradation on the sand–steel interface friction angle. J. Geotech. Geoenvironmental Eng. **144**, 04018096 (2018). https://doi.org/10.1061/(ASCE)GT.1943-5606.0001990
66. Uday, K.V., Padmakumar, G.P., Singh, D.N.: Some studies on morphology of the coarse-grained soils. Eng. Geol. **152**, 48–55 (2013). https://doi.org/10.1016/j.enggeo.2012.10.001
67. Suh, H.S., Kim, K.Y., Lee, J., Yun, T.S.: Quantification of bulk form and angularity of particle with correlation of shear strength and packing density in sands. Eng. Geol. **220**, 256–265 (2017). https://doi.org/10.1016/j.enggeo.2017.02.015
68. Choo, H., Kim, J., Lee, W., Lee, C.: Relationship between hydraulic conductivity and formation factor of coarse-grained soils as a function of particle size. J. Appl. Geophys. **127**, 91–101 (2016). https://doi.org/10.1016/j.jappgeo.2016.02.013
69. Çellek, S.: The effect of shape on the linear relationship of maximum and minimum void ratios of various sand types. Geotech. Geol. Eng. **37**, 3701–3713 (2019). https://doi.org/10.1007/s10706-019-00862-9
70. Guida, G., Sebastiani, D., Casini, F., Miliziano, S.: Grain morphology and strength dilatancy of sands. Géotech. Lett. **9**, 245–253 (2019). https://doi.org/10.1680/jgele.18.00199
71. Xiao, Y., Long, L., Matthew Evans, T., Zhou, H., Liu, H., Stuedlein, A.W.: Effect of Particle Shape on Stress-Dilatancy Responses of Medium-Dense Sands. J. Geotech. Geoenvironmental Eng. **145**, 04018105 (2019). https://doi.org/10.1061/(ASCE)GT.1943-5606.0001994
72. Sarkar, D., Goudarzy, M., König, D., Wichtmann, T.: Influence of particle shape and size on the threshold fines content and the limit index void ratios of sands containing non-plastic fines. Soils Found. **60**, 621–633 (2020). https://doi.org/10.1016/j.sandf.2020.02.006
73. Lashkari, A., Falsafizadeh, S.R., Shourijeh, P.T., Alipour, M.J.: Instability of loose sand in constant volume direct simple shear tests in relation to particle shape. Acta Geotech. (2020). https://doi.org/10.1007/s11440-019-00909-4
74. Krumbein, W.C., Sloss, L.L.: In: Freeman, W.H., & Co. (Ed) Stratigraphy and Sedimentation. SanFrancisco, 497 pp (1951)